Clifton, NJ, USA) with 0.1°C accuracy and a rectal probe for mice (RET-3, Physitemp Instrument Inc.). Each mouse was lightly restrained by hand for approximately 20 s while the probe was inserted approximately 2 cm into the rectum and a steady reading was obtained. Body temperature was measured rectally before and 15, 30, 45, and 60 min after intraperitoneal (i.p.) injection of MDMA (30 mg/kg) at an ambient temperature of 22 ± 2°C.

Drugs

MDMA was synthesized at Matsuyama University College of Pharmaceutical Sciences and freshly dissolved in saline. MDMA and vehicle were administered in a volume of 0.1 ml/10 g body weight.

Statistical Analysis

Mean and standard error were calculated from the values of 12-17 subjects. Changes in body temperature were analyzed by repeated-measures analysis of variance (ANOVA) followed by Scheffe's *post hoc* test. Baseline temperature and changes in body temperature areas-under-the-curve (AUC) were analyzed by one-way ANOVA and Scheffe's *post hoc* test.

RESULTS

Baseline Body Temperature in Parkin Knockout Mice

Baseline body temperature was measured before MDMA injection at room temperature (22 ± 2°C). No significant difference in baseline body temperature was observed among wildtype, heterozygous, and homozygous parkin knockout mice (Fig. **1**).

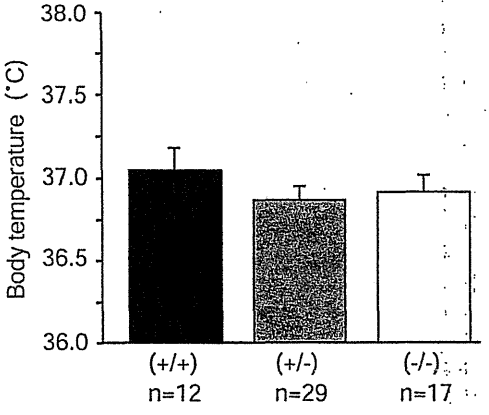

Fig. (1). No significant differences in baseline body temperature were observed among wildtype, heterozygous, and homozygous parkin knockout mice. Body temperature prior to MDMA injection did not significantly differ among genotypes. Baseline body temperature was analyzed by one-way ANOVA ($F_{2,55}$ = 0.629, p = 0.5369) at an ambient temperature of 22 ± 2°C.

No Sex Differences in MDMA-Induced Hyperthermia

Body temperature was measured 15, 30, 45, and 60 min after i.p. injection of MDMA (30 mg/kg) at an ambient temperature of 22 ± 2°C. No significant differences in MDMA-induced hyperthermia were observed between males and females within each genotype (Fig. **2**).

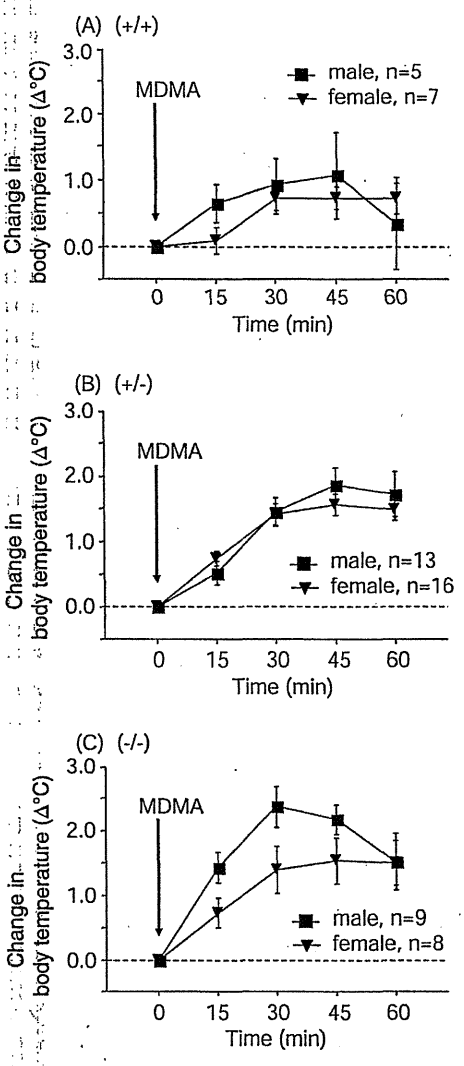

Fig. (2). Similar MDMA-induced (30 mg/kg, i.p.) hyperthermia was observed in male and female mice within each genotype. Body temperature areas-under-the-curve were analyzed by repeated-measures ANOVA. **(A)** Sex, $F_{1,10}$ = 0.181, p = 0.6796; Time, $F_{4,40}$ = 4.741, p = 0.0032; Sex × Time interaction, $F_{4,40}$ = 1.124, p = 0.3587. **(B)** Sex, $F_{1,27}$ = 0.134, p = 0.7170; Time, $F_{4,108}$ = 62.705, p < 0.0001; Sex × Time interaction, $F_{4,108}$ = 1.231, p = 0.3021. **(C)** Sex, $F_{1,15}$ = 2.350, p = 0.1461; Time, $F_{4,60}$ = 26.22, p < 0.0001; Sex × Time interaction, $F_{4,60}$ = 2.059, p = 0.0974.

Enhancement of MDMA-Induced Hyperthermia in Parkin Knockout and Heterozygous Mice

Body temperature gradually increased from baseline after MDMA injection in all genotype groups. MDMA significantly enhanced hyperthermia from 15 to 45 min after injection in parkin knockout mice and from 45 to 60 min after injection in heterozygous mice compared with wildtype mice (Fig. **3A**). MDMA produced hyperthermia, with a maximum increase of 0.9°C (37.9°C) 45 min after injection in wildtype mice, 1.7°C (38.6°C) 45 min after injection in heterozygous mice, and 1.9°C (38.8°C) 30 min after injection in parkin knockout mice. Body temperature AUC values reflected significantly enhanced hyperthermia in parkin knockout and heterozygous mice compared with wildtype mice (Fig. **3B**).

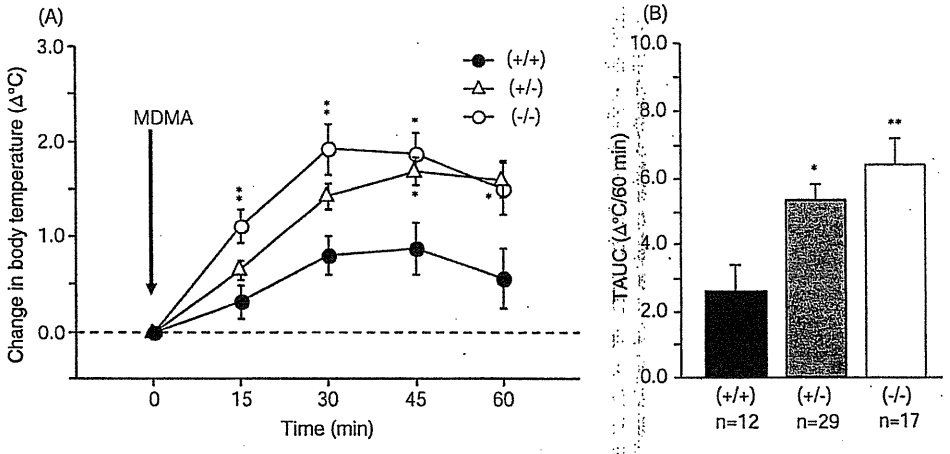

Fig. (3). Enhanced MDMA-induced hyperthermia in heterozygous and homozygous parkin knockout mice compared with wildtype mice. **(A)** Change in body temperature in mice injected with MDMA (30 mg/kg, i.p.). Body temperature areas-under-the-curve were analyzed by repeated-measures ANOVA (Genotype, $F_{2,55} = 6.746$, $p = 0.0024$; Time, $F_{4,220} = 61.267$, $p < 0.0001$; Genotype × Time interaction, $F_{8,220} = 3.664$, $p = 0.0005$) followed by Scheffe's *post hoc* test (*$p < 0.05$, **$p < 0.01$). **(B)** Change in body temperature areas-under-the-curve (TAUC) shown as an integration of the temperature *vs.* time curve shown in panel A. TAUC values were analyzed by one-way ANOVA ($F_{2,55} = 6.746$, $p = 0.0024$) followed by Scheffe's *post hoc* test (*$p < 0.05$, **$p < 0.01$).

DISCUSSION

In the present study, significantly enhanced MDMA-induced hyperthermia was observed in parkin knockout and heterozygous mice compared with wildtype mice (Fig. **3B**). The enhanced MDMA-induced hyperthermia in parkin knockout mice supports the hypothesis that parkin protects against MDMA-induced neurotoxic insult.

Hyperthermia is one of the major symptoms of acute MDMA-induced toxicity, which has been shown to be affected by body temperature [3]. MDMA produces a rapid enhancement of DA release in the striatum [1] and preoptic anterior hypothalamus [8]. MDMA-induced hyperthermia was blocked by a DA D_1 receptor antagonist [9]. Moreover, both the hyperthermia and augmented DA levels in the preoptic anterior hypothalamus after i.p. MDMA injection were significantly reduced by pretreatment with a D_1 antagonist [8]. Interestingly, Sato *et al.* (2006) [10] reported that D_1 receptor levels in the striatum in parkin knockout mice was higher than in wildtype mice, although no change in TH-positive substantia nigra neurons was found in parkin knockout mice, and no significant decrease in DAT levels was observed in the striatum. Therefore, the enhanced MDMA-induced hyperthermia observed in the present study may be attributable to increased levels of D_1 receptors in parkin knockout mice.

Sato *et al.* (2006) [10] also suggested that presynaptic neurons (i.e., DAergic neurons) are functionally impaired in parkin knockout mice. DA synthesis is significantly decreased and methamphetamine-induced DA release is reduced in parkin knockout mice. Considering that DAergic neurons in the substantia nigra are severely damaged in PD patients, the enhanced MDMA-induced hyperthermia in parkin knockout mice may be attributable to functional impairment of DAergic neurons, although the relationship between hyperthermia and DAergic neuron dysfunction remains to be elucidated.

Additionally, we found no significant difference in baseline body temperature among wildtype, heterozygous, and homozygous parkin knockout mice (Fig. **1**). These data suggest that parkin does not play a crucial role in the system that maintains basal body temperature.

In conclusion, MDMA-induced hyperthermia was enhanced in parkin knockout and heterozygous mice compared with wildtype mice. Parkin is hypothesized to be critical for protecting DAergic neurons from toxic insult, and the present results suggest that parkin plays a protective role against MDMA-induced DAergic neuron neurotoxicity.

ACKNOWLEDGEMENTS

We acknowledge Mr. Michael Arends for his assistance with editing the manuscript and Ms. Junko Hasegawa for her assistance with genotyping mice. This work was supported by a research grant (17025054) from the MEXT of Japan, by grants from the MHLW of Japan (H17-pharmaco-001, H19-iyaku-023, and 18A-3 and 19A-8 for Nervous and Mental Disorders), by a grant from the Smoking Research Foundation, and by a grant from the Mitsubishi Foundation for Social Welfare Activities.

ABBREVIATIONS

ANOVA	=	Analysis of variance
DA	=	Dopamine
DAT	=	Dopamine transporter
MDMA	=	3,4-methylenedioxymethamphetamine
PD	=	Parkinson's disease
TH	=	Tyrosine hydroxylase

REFERENCES

[1] Camarero, J.; Sanchez, V.; O'Shea, E.; Green, A.R.; Colado, M.I. Studies, using *in vivo* microdialysis, on the effect of the dopamine uptake inhibitor GBR 12909 on 3,4-methylenedioxymethamphetamine ("ecstasy")-induced dopamine release and free radical formation in the mouse striatum. *J. Neurochem.*, **2002**, *81*, 961-972.

[2] Doly, S.; Valjent, E.; Setola, V.; Callebert, J.; Hervé, D.; Launay, J.M.; Maroteaux, L. Serotonin 5-HT_{2B} receptors are required for

3,4-methylenedioxymethamphetamine-induced hyperlocomotion and 5-HT release *in vivo* and *in vitro*. *J. Neurosci.*, **2008**, *28*, 2933-2940.

[3] Colado, M.I.; Camarero, J.; Mechan, A.O.; Sanchez, V.; Esteban, B.; Elliott, J.M.; Green, A.R. A study of the mechanisms involved in the neurotoxic action of 3,4-methylenedioxymethamphetamine (MDMA, "ecstasy") on dopamine neurones in mouse brain. *Br. J. Pharmacol.*, **2001**, *134*, 1711-1723.

[4] Granado, N.; O'Shea, E.; Bove, J.; Vila, M.; Colado, M.I.; Moratalla, R. Persistent MDMA-induced dopaminergic neurotoxicity in the striatum and substantia nigra of mice. *J. Neurochem.*, **2008**, *107*, 1102-1112.

[5] Malberg, J.E.; Seiden, L.S. Small changes in ambient temperature cause large changes in 3,4-methylenedioxymethamphetamine (MDMA)-induced serotonin neurotoxicity and core body temperature in the rat. *J. Neurosci.*, **1998**, *18*, 5086-5094.

[6] Shimura, H.; Hattori, N.; Kubo, S.; Mizuno, Y.; Asakawa, S.; Minoshima, S.; Shimizu, N.; Iwai, K.; Chiba, T.; Tanaka, K.; Suzuki, T. Familial Parkinson disease gene product, parkin, is a ubiquitin-protein ligase. *Nat. Genet.*, **2000**, *25*, 302-305.

[7] Xu, J.; Kao, S.Y.; Lee, F.J.; Song, W.; Jin, L.W.; Yankner, B.A. Dopamine-dependent neurotoxicity of α-synuclein: a mechanism for selective neurodegeneration in Parkinson disease. *Nat. Med.*, **2002**, *8*, 600-606.

[8] Benamar, K.; Geller, E.B.; Adler, M.W. A new brain area affected by 3,4-methylenedioxymethamphetamine: a microdialysis-biotelemetry study. *Eur. J. Pharmacol.*, **2008**, *596*, 84-88.

[9] Mechan, A.O.; Esteban, B.; O'Shea, E.; Elliott, J.M.; Colado, M.I.; Green, A.R. The pharmacology of the acute hyperthermic response that follows administration of 3,4-methylenedioxymethamphetamine (MDMA, "ecstasy") to rats. *Br. J. Pharmacol.*, **2002**, *135*, 170-180.

[10] Sato, S.; Chiba, T.; Nishiyama, S.; Kakiuchi, T.; Tsukada, H.; Hatano, T.; Fukuda, T.; Yasoshima, Y.; Kai, N.; Kobayashi, K.; Mizuno, Y.; Tanaka, K.; Hattori, N. Decline of striatal dopamine release in parkin-deficient mice shown by *ex vivo* autoradiography. *J. Neurosci. Res.*, **2006**, *84*, 1350-1357.

Received: October 01, 2009 Revised: April 17, 2010 Accepted: May 26, 2010

Neurobiology of Disease 43 (2011) 651–662

Contents lists available at ScienceDirect

Neurobiology of Disease

journal homepage: www.elsevier.com/locate/ynbdi

DJ-1 associates with synaptic membranes

Yukiko Usami [a], Taku Hatano [a], Satoshi Imai [b,1], Shin-ichiro Kubo [a], Shigeto Sato [a], Shinji Saiki [a], Yoichiro Fujioka [c], Yusuke Ohba [c], Fumiaki Sato [b,2], Manabu Funayama [a,b], Hiroto Eguchi [a], Kaori Shiba [b], Hiroyoshi Ariga [d], Jie Shen [e], Nobutaka Hattori [a,b,*]

[a] *Department of Neurology, Juntendo University School of Medicine, Japan*
[b] *Research Institute for Diseases of Old Age, Graduate School of Medicine, Juntendo University, Japan*
[c] *Laboratory of Pathophysiology and Signal Transduction, Hokkaido University Graduate School of Medicine, Japan*
[d] *Graduate School of Pharmaceutical Sciences, Hokkaido University, Japan*
[e] *Center for Neurologic Diseases, Brigham and Women's Hospital Program in Neuroscience, Harvard Medical School, USA*

ARTICLE INFO

Article history:
Received 6 February 2011
Revised 30 April 2011
Accepted 20 May 2011
Available online 30 May 2011

Keywords:
DJ-1
Parkinson's disease
Localization
Synaptic vesicles
Synaptophysin
VAMP2
Rab3A

ABSTRACT

Parkinson's disease (PD) is a neurodegenerative disorder caused by loss of dopaminergic neurons. Although many reports have suggested that genetic factors are implicated in the pathogenesis of PD, molecular mechanisms underlying selective dopaminergic neuronal degeneration remain unknown. *DJ-1* is a causative gene for autosomal recessive form of *PARK7*-linked early-onset PD. A number of studies have demonstrated that exogenous DJ-1 localizes within mitochondria and the cytosol, and functions as a molecular chaperon, as a transcriptional regulator, and as a cell protective factor against oxidative stress. However, the precise subcellular localization and function of endogenous DJ-1 are not well known. The mechanisms by which mutations in DJ-1 contributes to neuronal degeneration also remain poorly understood. Here we show by immunocytochemistry that DJ-1 distributes to the cytosol and membranous structures in a punctate appearance in cultured cells and in primary neurons obtained from mouse brain. Interestingly, DJ-1 colocalizes with the Golgi apparatus proteins GM130 and the synaptic vesicle proteins such as synaptophysin and Rab3A. Förster resonance energy transfer analysis revealed that a small portion of DJ-1 interacts with synaptophysin in living cells. Although the wild-type DJ-1 protein directly associates with membranes without an intermediary protein, the pathogenic L166P mutation of DJ-1 exhibits less binding to synaptic vesicles. These results indicate that DJ-1 associates with membranous organelles including synaptic membranes to exhibit its normal function.

Introduction

Parkinson's disease (PD) is the second most common neurodegenerative disorder next to Alzheimer's disease and is characterized by motor symptoms as cardinal features such as resting tremor, rigidity, bradykinesia and postural instability. Pathological hallmarks of PD include marked cell loss of dopaminergic neurons in the substantia nigra pars compacta which causes dopamine depletion in the striatum and the presence of intracytoplasmic inclusions known as Lewy bodies in the remaining neurons (Fearnley and Lees, 1991). Although most of the PD cases are sporadic, approximately 5% of PD patients have clear familial etiology. Thus, the presence of monogenic forms of familial PD tells us that genetic factors contribute to the pathogenesis of PD. Indeed, heterozygous and homozygous mutations in one of the responsible genes have been reported in sporadic cases, suggesting that genetic factors are implicated in the pathogenesis of PD. Until now, 9 genes for familial PD have been reported, and these include *α-synuclein*, *parkin*, *UCH-L*, *PINK-1*, *DJ-1*, *LRRK2*, *ATP13A2*, *PLA2G6*, and *FBXO7* (Hatano et al., 2009).

Previous reports have suggested that DJ-1 functions as a molecular chaperon (Lee et al., 2003), a transcriptional regulator (Kim et al., 2005; Niki et al., 2003; Shinbo et al., 2005; Takahashi et al., 2001), and as a cell protective factor against oxidative stress (Canet-Aviles et al., 2004; Taira et al., 2004b; Yokota et al., 2003). The localization of DJ-1 has been shown to be in mitochondria, cytosol, nucleus, and microsomes (endoplasmic reticulum (ER) and Golgi) (Bonifati et al., 2003; Canet-Aviles et al., 2004; Miller et al., 2003; Taira et al., 2004a). However, most studies have been performed by exogenous DJ-1 using overexpression systems. On the other hand, endogenous DJ-1 is present in synaptic terminals, in both axons and dendrites, as well as

Abbreviations: PD, Parkinson's disease; FRET, Förster resonance energy transfer; WT, wild type; ER, endoplasmic reticulum; KO, knockout; RT, room temperature; PBS, phosphate-buffer saline; FBS, fetal bovine serum; BSA, bovine serum albumin; Tfn-R, transferrin receptor; IR, immunoreactivity; HB, homogenizing buffer.

* Corresponding author at: Department of Neurology, Juntendo University School of Medicine, 2-1-1 Hongo, Bunkyo-ku, Tokyo 113-8421, Japan. Fax: +81 3 5800 0547.
E-mail address: nhattori@juntendo.ac.jp (N. Hattori).
[1] Present affiliation: Department of Toxicology, School of Pharmacy and Pharmaceutical Sciences, Hoshi University, Japan.
[2] Present affiliation: Department of Clinical Chemistry, School of Pharmacy and Pharmaceutical Sciences, Hoshi University, Japan.

Available online on ScienceDirect (www.sciencedirect.com).

0969-9961/$ – see front matter © 2011 Elsevier Inc. All rights reserved.
doi:10.1016/j.nbd.2011.05.014

in mitochondria (Olzmann et al., 2007; Zhang et al., 2005). However, the precise function and dynamics of DJ-1 related to vesicular trafficking remain unclear: In the present study, we demonstrate the association of endogenous DJ-1 with membranous organelles and the molecular interaction of recombinant DJ-1 protein with membranes in cultured cells. In addition, we examine whether pathogenic mutations found in *PARK7*-linked early onset PD patients may be affected by binding activities of DJ-1.

Materials and methods

Antibodies and recombinant proteins

Mouse monoclonal antibody (M043-3, Clone 3E8) and rabbit polyclonal antibody (NB300-270) for DJ-1 were obtained from Medical & Biological Laboratories Co. (MBL, Nagoya, Japan) and Novus Biologicals, Inc. (Littleton, CO), respectively. Rabbit polyclonal antibodies to Rab3A (sc-308), Rab4A (sc-312), Rab5B (sc-598), and Tom20 (sc-11415) were purchased from Santa Cruz Biotechnology (Santa Cruz, CA), and Rab7B (R4779) was obtained from Sigma (St. Louis, MO). Mouse monoclonal antibodies to synaptophysin were purchased from Chemicon International, Inc. (MAB5258, Temecula, CA) (used for immunoblotting) and Progen Biotechnik (61012, Heidelberg, Germany) (used for immunocytochemistry). Synaptotagmin (610434) and NMDAR1 (556308) were obtained from BD Biosciences Pharmingen (San Diego, CA). Other primary antibodies were Rab3A (107111, Synaptic Systems, Gottingen, Germany), anti-human transferrin receptor (13-6800, Zymed Laboratories, South San Francisco, CA), Parkin (#4211) and Calnexin (#2679S) (Cell Signaling, Danvers, MA), VAMP2 (NB300-595, Novus Biologicals, Inc.), BIP2 (ab21685, Abcam, Cambridge, MA), Hsp70 (610608, BD Transduction Laboratories), Mito Tracker Red CMXRos (M-7512, Molecular Probes), and total OXPHOS rodent WB antibody cocktail (MS604; MitoSciences, Eugene, Oregon). Secondary antibodies conjugated to horseradish peroxidase were purchased from GE HealthCare Bio-Sciences (Piscataway, USA). From Invitrogen Molecular Probes, 488 and 546 conjugated secondary antibodies were purchased. The vectors encoding GST-tagged WT and mutants DJ-1 (M26I, A104T, D149A, and L166P) were kindly provided by Hiroyoshi Ariga (Laboratory of Pharmaceutical Science, Hokkaido University).

Experimental animals (DJ-1 KO mice)

The DJ-1 KO mice (F2) were a kind gift from The Laboratory of Pharmaceutical Science, Hokkaido University. The DJ-1 KO mice were generated at the Center for Neurologic Diseases, Brigham and Women's Hospital Program in Neuroscience, Harvard Medical School (Goldberg et al., 2005). F2 progeny were backcrossed for five generations to C57BL/6 mice, and heterozygotes were intercrossed to generate homozygous mice for the targeted *DJ-1* allele. For the experiments, C57BL/6J mice and DJ-1 KO mice were used at 7 to 9 weeks of age. All animal experiments were carried out in accordance with the Ethics Review Committee for Animal Experimentation of Juntendo University School of Medicine.

Cell culture and transfection

SH-SY5Y cells and HeLa cells were grown in Dulbecco's modified Eagle's medium (D-MEM, Sigma) with 10% fetal bovine serum (FBS; Sigma) and 1% penicillin–streptomycin (PS; Invitrogen). SH-SY5Y cell culture medium was supplemented with 1% non-essential amino acid, 1% sodium pyruvate, and 1% L-glutamate (Invitrogen). The cells were cultured at 37 °C and 5% CO_2. PC12 cells were grown in D-MEM with 5% FBS and 10% horse serum. Primary cortical neurons containing glia cells were prepared from E15.5 C57BL/6J mice and cultured for growth on Fisher-brand cover glass (Fisher Scientific, Pittsburgh, USA) in starting medium (F12 and Minimum Essential Medium with 10% FBS, 1% PS, and 0.001% insulin) for 3 days, and incubated sequentially for 5 days with 0.5 μM Ara-C (Sigma) in maintenance medium (F12 and Minimum Essential Medium with 5% calf serum, 5% horse serum, 1% PS, and 0.001% insulin). HeLa cells were transfected with expression vectors for FLAG-DJ-1 WT, M26I, A104T, D149A, or L166P by using FuGENE HD Transfection Reagent (Roche). After 24 h, immunocytochemistry was performed on the cells.

Immunocytochemistry

Cells were fixed for 10 min in 4% paraformaldehyde and 0.5% sucrose in phosphate-buffered saline (PBS). The cells were permeabilized with PBS containing 0.2% Triton X-100 (Sigma) for 5 min at RT. For blocking, 1× BlockAce (Yukijirushi Co., Osaka, Japan) was used for SH-SY5Y cells, and 10% FBS and 1% bovine serum albumin (BSA) in PBS (primary cortical neurons from mice) was used for primary cortical neurons for 30 min. Cells were incubated overnight with primary antibodies at 4 °C. The cells were washed 3 times with PBS and were incubated at RT for 1 h with secondary antibodies. After the cells were washed 3 times with PBS, the slides were mounted with Vectashield (Vector Laboratories, Burlingame, CA) and analyzed using a Leica confocal microscopy.

Preparation of synaptosome fractions from mouse brain

Synaptic vesicles were prepared as described previously (Hatano et al., 2007; Hell, 1998), with some modification. Briefly, whole brains from 3 mice (C57BL/6J) at 7 to 9 weeks of age were placed into 8 ml ice-cold synaptosomal homogenizing buffer (HB) (0.32 M sucrose, 4 mM HEPES–NaOH, pH 7.4 with EDTA-free protease inhibitor cocktail Complete Mini, EDTA free). The tissues were homogenized using a glass-Teflon homogenizer (10 up and down strokes, 830 rpm). The homogenized brain sample was centrifuged at 1000g for 10 min at 4 °C. After the supernatant (S1-1) was removed, the pellet was re-suspended in 5 ml HB and was homogenized and centrifuged at the same speed. The supernatant (S1-2) was removed, and the pellet was resuspended in 3 ml HB, and was homogenized and centrifuged in the same manner. The pellet was considered the P1 fraction, while the supernatant (mixed with S1-1, S1-2, and S1-3) was centrifuged at 12,000g for 15 min at 4 °C. The supernatant (S2) was removed and the pellet (P2) was resuspended with HB, and then centrifuged for 15 min at 13,000g at 4 °C. After removal of the supernatant (S2′), the pellet (P2′) was collected as the crude synaptosome fraction. P2′ was subsequently re-suspended with HB to a final volume of 1 ml. The P2′ fraction was suspended with 4 ml of ice cold water in the EDTA-free protease inhibitor cocktail. The samples were homogenized by 6 up and down strokes of the glass-Teflon homogenizer at 830 rpm and mixed with 39 μl 1 M HEPES, pH 7.4, then centrifuged for 20 min at 33,000g at 4 °C. The lysate pellet was considered the LP1 fraction, and the supernatant (LS1) was centrifuged for 2 h at 260,000g at 4 °C. After the supernatant (LS2) was removed, the pellet (LP2) was resuspended with 300 μl of HB. To loosen the pellet, samples were extruded consecutively through a 23-gauge and a 26-gauge hypodermic needle attached to a 1 ml syringe. The concentration of protein in each of the fractions was calculated using the BCA protein assay kit (Pierce, Rockford, IL). Finally, the same amounts of proteins from each fraction were analyzed by SDS–PAGE followed by immunoblotting.

Sucrose gradients of LS1 fraction from mouse brain

The LS1 fraction was layered on top of a linear sucrose density gradient ranging from 0.2 to 2.0 M sucrose dissolved in HEPES buffer (pH 7.4), and ultra-centrifuged at 465,000g for 13 h at 4 °C. Each of the fractions (0.5 ml) was collected from the top of the gradient, and equal volumes of each fraction were subjected to SDS–PAGE followed by immunoblotting.

Preparation of magnetic beads cross-linked with antibodies

For the following experiments of immunoisolation and immunoprecipitation, the DJ-1 polyclonal antibody and the synaptophysin antibody, and the normal rabbit IgG and the normal mouse IgG as control, were cross-linked to protein G-coated magnetic beads (Dynabeads Invitrogen). The beads were washed 3 times with citrate buffer, and then 50 μl of magnetic bead slurry was combined with 50 μg of each antibody by rotating for 1 h at RT. The antibody-bound beads were washed 3 times with 0.2 M sodium borate buffer (pH 9.0), and then resuspended in 0.2 M sodium borate buffer containing dimethyl pimelimidate (Pierce Biotechnology). After reacting by rotating the samples for 1 h at RT, the supernatants were removed and the Dynabead pellets were washed 3 times with 0.2 M triethanolamine buffer (pH 8.0). The washed beads were suspended with 0.2 M triethanolamine buffer containing 50 mM glycine, and were reacted for 2 h at RT. The supernatant was removed and the beads were washed 3 times with PBS, stored at 4 °C with PBS containing 0.05% Tween 20, and used within 1 week of the reactions.

Immunoisolation and immunoprecipitation of LS1 fraction containing synaptic vesicles from the mouse brain

Immunoisolation: beads cross-linked with DJ-1 antibody and synaptophysin antibody, or beads cross-linked with normal rabbit IgG and normal mouse IgG were washed 6 times with PBS and were blocked for 1 h at RT using PBS containing 10% BSA as nonspecific competitor, followed by washing in PBS 3 times. In addition, each of the 1 ml LS1 fraction samples were immunoisolated with 37.5 μl of the beads cross-linked with antibody for a total of 12 h at 4 °C after blocking non-specific sites by rotating with the beads with the cross-linked normal rabbit IgG, or normal mouse IgG for 1 h at 4 °C. The pellets and supernatants were subjected to SDS–PAGE followed by immunoblotting using antibodies against the indicated proteins.

Immunoprecipitation: beads cross-linked with the antibodies, the same as in the immunoisolation protocol, were blocked using PBS containing 10% BSA for 1 h at RT. LS1 fractions (900 μl) were dissolved in 100 μl of 10× RIPA buffer (final concentration: 140 mM KCl, 20 mM HEPES–KOH (pH 7.3), 2 mM EDTA, protease inhibitors, and 1% Triton X-100), and then the samples were blocked by rotating with normal IgG for 1 h at 4 °C. The supernatants were immunoprecipitated with 12.5 μl of each of the beads cross-linked with antibody overnight at 4 °C. The pellets and supernatants were subjected to SDS–PAGE followed by immunoblotting using antibodies against the indicated proteins.

Förster resonance energy transfer (FRET)

Synaptophysin-YFP and pCAGGS-CFP vector were a kind of gift from the Department of Cellular Neurobiology Graduate School of Medicine University of Tokyo. CFP–DJ-1 and CFP–VAMP2 were generated by fusing in frame to the DJ-1 N-terminal or VAMP2 N-terminal coding region in the pCAGGS-CFP vector. HeLa cells were transfected with expression vectors for CFP–DJ-1 or CFP–VAMP2, and synaptophysin-YFP using FuGene HD (Roche), according to the manufacturer's instruction. After 24 h, the cells were imaged with an IX70 inverted microscope (Olympus, Tokyo, Japan) equipped with BioPoint MAC5000 excitation and emission filter wheels (Ludl Electronic Products Ltd., Hawthorne, NY) and a Cool SNAP-HQ cooled CCD camera (Roper Scientific, Trenton, NJ). The filters used were purchased from Omega Optical Inc. (Brattleboro, VT): two excitation filters, XF1071 (440AF21) for CFP and Förster resonance energy transfer (FRET), and XF1068 (500AF25) for YFP; an XF2034 (455DRLP) dichroic mirror; two emission filters, XF3075 (480AF30) for CFP and XF3079 (535AF26) for FRET and YFP. Cells were illuminated with a 75 W xenon lamp through a 6% ND filter. Exposure times for 3×3 binning were 100 ms to obtain fluorescence images and 20 ms to obtain differential interference contrast image. MetaMorph software (Universal Imaging, West Chester, PA) was used to control the CCD camera and filter wheels, and also for the analysis of the cell image data.

Sensitized FRET measurement was performed using the method by Gordon et al.(1998). Briefly, fluorescence images for more than 20 cells were acquired sequentially through YFP, CFP, and FRET filter channels. The background was subtracted from raw images before FRET calculations. The fractions of the bleed-through of CFP and YFP fluorescence through the FRET channel were 0.502 and 0.385, respectively. Corrected FRET ($FRET_C$) was therefore calculated on a pixel-by-pixel basis for the entire image by using the equation: $FRET_C = FRET - 0.502 \times CFP - 0.385 \times YFP$, where FRET, YFP, and CFP correspond to background-subtracted images of cells co-expressing CFP and YFP. Calculated $FRET_C$ values are expressed as box and whisker plots, where the highest and lowest boundaries of the box represent the 25th and 75th percentiles, respectively, and whiskers above and below the box designate the 10th and 90th percentiles, respectively; the line within the box indicates the median value. $FRET_C$ images are also presented in the pseudocolor mode.

Alternatively, 293F cells (Invitrogen) were transfected with expression vectors for CFP–DJ-1 or CFP–VAMP2, and synaptophysin-YFP using 293fectin (Invitrogen) according to the manufacturer's recommendation. After 24 h, the cells were analyzed by a Flicyme-300 flow cytometer (Mitsui engineering and Shipment, Tokyo, Japan), which is equipped with a 445 nm semiconductor laser and is able to measure the fluorescence lifetime of CFP in the frequency domain at a single cell level. Data were acquired using the machine-bundled software, and exported to FlowJo flow cytometry analysis software (Tree Star, Inc., Ashland, OR). Using a gate tool, a population that expresses both CFP and YFP was selected, and FRET efficiency (E) of each cell was calculated by the following equation: $E = 1 - \tau_d'/\tau_d$, where, τ_d' and τ_d are donor (CFP) lifetimes in the presence and absence of the acceptor chromophore, respectively. E values of all analyzed cells were plotted in box and whisker plots.

Confocal laser scanning microscopy

Confocal images were obtained using an FV-10i confocal microscope (Olympus, Tokyo, Japan). Image data were exported to MetaMorph software and fluorescence intensities on lines of interest were gauged by the "Line Scan" function and plotted.

Cell fractionation

For cell fractionation studies, cultured cells (PC12) were washed with PBS, scraped off the culture plate in PBS, and centrifuged at 600*g* for 5 min. Cell pellets were resuspended in homogenization buffer (20 mM HEPES pH 7.2 and 0.25 M sucrose) in the presence of a cocktail of protease inhibitor (Complete Mini, EDTA-free), and sonicated at 4 °C (10 s, 3 times). The nuclei and unbroken cells were then pelleted by centrifugation at 1000*g* for 10 min at 4 °C. The supernatant was centrifuged at 100,000*g* for 1 h at 4 °C to separate the cytosolic and membrane fractions. To study the effects of salts and non-ionic detergent on the solubilization of DJ-1, the membrane fractions were incubated on ice for 30 min with homogenization buffer with 50, 150, and 1000 mM sodium chloride or 1% Triton X-100. After separation of the soluble and insoluble materials by centrifugation (100,000*g*, for 1 h, at 4 °C), equal volumes of each fraction were subjected to immunoblot with DJ-1, Parkin, and Tfn-R antibodies.

Proteinase K (PK) digestion of PC12 cell membrane fractions

Membrane fractions were isolated from PC12 cells and incubated with 0, 20, 40, 60, 80, and 120 μl of Proteinase K (PK)-agarose (Sigma) at 30 °C with rotation for 1 h. PK beads were removed from the

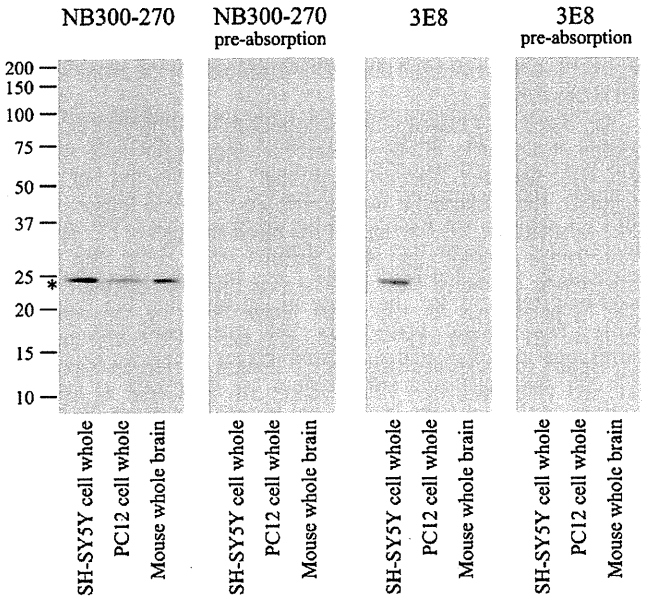

Fig. 1. Characterization of anti-DJ-1 antibodies. (A) Immunoblot of lysates from SH-SY5Y cells, PC12 cells, and mouse whole brain. Commercially available DJ-1 rabbit polyclonal antibody and mouse monoclonal antibody were used, as mentioned in Materials and methods. Specificities of these antibodies were confirmed by pre-absorption tests.

reacted membrane by centrifugation 5 times. PK-treated membranes were subjected to electrophoresis through Tris–HCl polyacrylamide gels (BIO-CRAFT) followed by staining with the GelCode SilverSNAP Stain Kit (Pierce).

In vitro binding assay by PC12 membranes

Recombinant DJ-1 WT, fused at its N terminus to the GST protein, or GST protein for negative control, were reacted with PC12 membranes, or PK-treated membranes (120 μl of PK beads concentration), at 30 °C for 1 h. The reacted samples were centrifuged at 100,000*g* for 1 h at 4 °C, and divided into supernatant and pellet. Both supernatant and pellet were subjected to SDS–PAGE followed by immunoblotting.

In vitro binding assay by LS1 fraction from DJ-1 KO mice

GST–DJ-1 WT recombinant protein (500 nM) or GST–DJ-1 mutant recombinant protein (M26I, A104T, D149A, and L166P) were combined with 200 μl of the LS1 fraction from DJ-1 KO mice ($n=3$), and rotated at 30 °C for 20 min. After treatment, the samples were centrifuged at 260,000*g* for 2 h at 4 °C. The supernatants were extracted and equal volumes of each fraction were subjected to immunoblot with anti-GST antibodies. The pellets were resuspended with the buffer (0.32 M sucrose-HEPES (pH 7.4) buffer) of equal volume, and equal volumes of each fraction were also subjected to immunoblot.

Immunoblotting

Cell lysates were mixed with LDS sample buffer (Invitrogen), heated for 5 min at 95 °C, and incubated on ice. The samples were resolved on 10–20% Tris–HCl gel (BIO CRAFT) in 1% SDS buffer and transferred onto polyvinylidene fluoride membranes (Bio-Rad Bioscience; Hercules, CA). The membranes were blocked for 1 h in TBS containing 0.1% Tween-20 (TBS-T) and 5% non-fat milk (BD Disco), and then incubated overnight at 4 °C with the primary antibody. The membranes were washed with TBS-T 3 times, followed by incubation for 1 h at RT with horseradish peroxidase-conjugated anti-mouse or anti-rabbit IgG. Immunoreactivity (IR) was assessed by a chemiluminescence reaction using Western Lightning (Perkin Elmer-Cetus, Foster City, CA) or ECL Plus reagent (GE Health Care Bio-Sciences).

Results

Characterization of anti-DJ-1 antibodies

To determine the endogenous localization of DJ-1, we employed the use of the commercially available mouse monoclonal and rabbit polyclonal DJ-1 antibodies. Immunoblot analyses using NB300-270 antibody (a rabbit polyclonal antibody) revealed a single band around 22 kDa corresponding to endogenous DJ-1 in the extracts from SH-SY5Y cells, PC12 cells, and mouse brain (Fig. 1). The 3E8 antibody, a mouse monoclonal antibody, also recognized a single band corresponding to the human DJ-1 protein in SH-SY5Y cells. However, this antibody did not detect the rodent DJ-1 protein in PC12 cells and mouse brain (Fig. 1). The band corresponding to DJ-1 disappeared when the antibody was pre-incubated with an excess amount of the antigen, confirming the specificity of the antibody (Fig. 1). Based on these results, the 3E8 antibody, which specifically recognizes endogenous human DJ-1, was used for immunocytochemistry, and the polyclonal NB300-270 antibody, which recognizes the mouse and rodent DJ-1 protein, was used for immunoblotting and immunocytochemistry of primary cortical neuronal cells obtained from mouse brain.

DJ-1 diffusely distributes with main membranous organelles

To examine the subcellular localization of DJ-1, SH-SY5Y cells were double-stained with the DJ-1 antibody and organelle-specific antibodies. Microscopic observation revealed diffuse DJ-1 immunostaining and the protein partly colocalized with GM130, a marker for Golgi apparatus. A small portion of DJ-1 colocalized with Mito Tracker and Tom20, both mitochondrial markers, and calnexin, an ER marker (Fig. 2A).

Based on the immunocytochemical data showing diffuse distribution of DJ-1 in cultured cells, we investigated the precise localization of DJ-1 using biochemical methods. To elucidate DJ-1 distribution in neuronal cells, mouse brain samples were fractionated by differential centrifugation and the fractions were analyzed for the presence of DJ-1 by immunoblotting (Fig. 2B). DJ-1 was present at considerable levels in the synaptosomes (P2′), which consisted of synaptic terminals including synaptic plasma membranes (LP1) and synaptic vesicles (LP2), and co-fractionated with synaptophysin, synaptotagmin, and

Fig. 2. DJ-1 was widely distributed with the main membranous organelles and synaptosomes. (A) SH-SY5Y cells were double-stained with antibodies to DJ-1 (green) and Mito Tracker, Tom20 (mitochondria), GM130 (Golgi apparatus), or calnexin (ER). Scale bars = 10 μm. (B) The experimental design of the synaptosome preparation is shown. (C) Subcellular fractionation of the mouse brain is described in Materials and methods. Aliquots of the subcellular fractions, containing 5 μg of protein, were analyzed by immunoblotting. NR-1 (membrane marker) was recognized in the LP1 fraction, and synaptophysin, synaptotagmin, and VAMP2 (vesicle marker) were detected in the LP2 fraction. Rab3A, Rab4A, Rab5B and Rab7B were widely concentrated in various subcellular fractions. DJ-1 was found in various fractions in conjunction with the Rab proteins. (D) Complex I–V (mitochondria), and GM130 (Golgi apparatus) organelle markers were investigated. Mitochondria were present in the P2′ and the LP1 fractions, but mitochondria were barely evident in the synaptic fraction. The Golgi fraction did appear in the cytosolic fraction (S2). (E) The amount of each fraction was quantified and graphed as a percentage for the estimated amount of whole brain protein. Data were the average ± SD of three independent experiments. (F) Using the results from panel C, immunoreactivity (IR) of each fraction was quantified and graphed as a percentage of each IR to the total immunoreactivities in DJ-1. Synaptophysin and NR-1 were compared with DJ-1 as well.

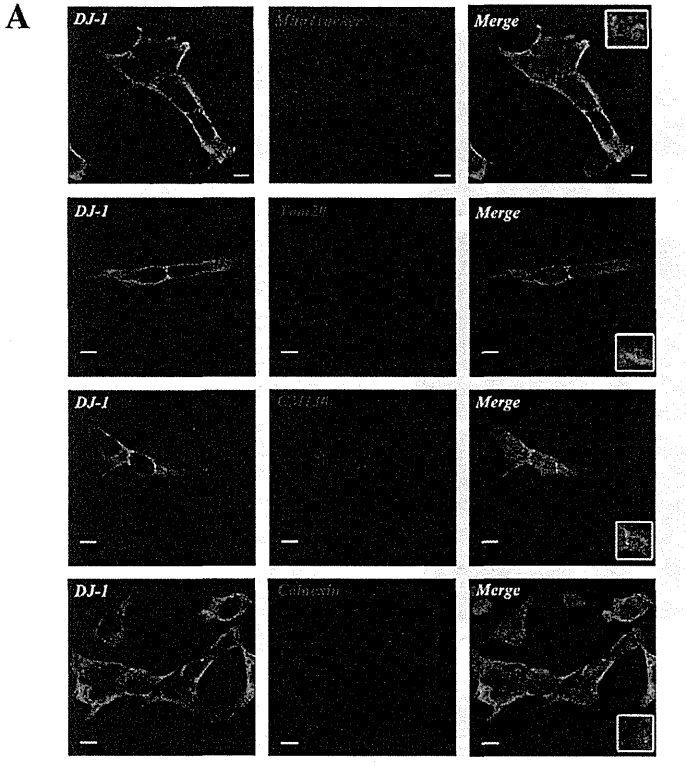
A
DJ-1
Merge
DJ-1
Merge
DJ-1
Merge
DJ-1
Merge
B
Mouse whole brain (n=3)
320 mM Sucrose
4 mM HEPES
Comp mini tab 1tab/10ml
Homogenization
1,000 x g, 10 min
Supernatant (S1)
Pellet (P1)
12,000 x g, 15 min
Supernatant (S2)
Pellet (P2)
13,000 x g, 15 min
Supernatant (S2')
Pellet
DDW
Homogenization (P2')
33,000 x g, 20 min
Supernatant
Pellet (LP1)
(Sinaptic cytosol + vesicle, LS1)
260,000 x g, 2 hr
Supernatant (LS2)
Pellet (LP2)
P1
S1
P2'
LS2
LP1
LP2

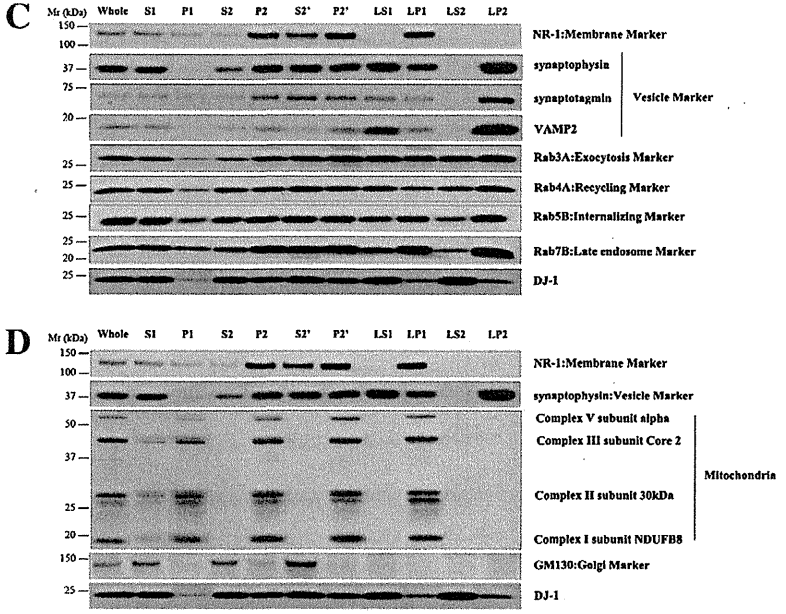
C
Mr (kDa)
Whole
S1
P1
S2
P2
S2'
P2'
LS1
LP1
LS2
LP2
NR-1:Membrane Marker
synaptophysin
synaptotagmin
Vesicle Marker
VAMP2
Rab3A:Exocytosis Marker
Rab4A:Recycling Marker
Rab5B:Internalizing Marker
Rab7B:Late endosome Marker
DJ-1
D
Mr (kDa)
Whole
S1
P1
S2
P2
S2'
P2'
LS1
LP1
LS2
LP2
NR-1:Membrane Marker
synaptophysin:Vesicle Marker
Complex V subunit alpha
Complex III subunit Core 2
Complex II subunit 30kDa
Complex I subunit NDUFB8
Mitochondria
GM130:Golgi Marker
DJ-1

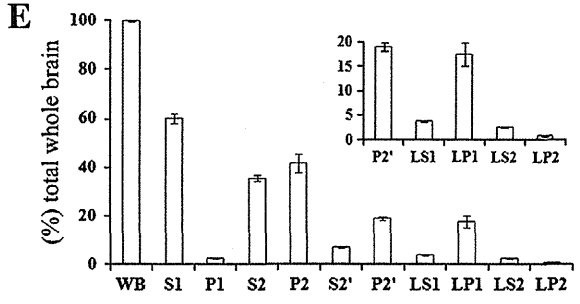
E
(%) total whole brain
WB
S1
P1
S2
P2
S2'
P2'
LS1
LP1
LS2
LP2

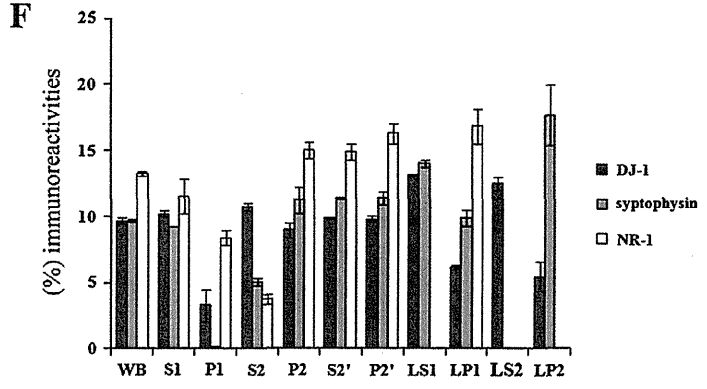
F
(%) immunoreactivities
DJ-1
syptophysin
NR-1
WB
S1
P1
S2
P2
S2'
P2'
LS1
LP1
LS2
LP2

VAMP2 (Fig. 2C). To further characterize the distribution of DJ-1 within synaptosomes, we investigated members of the family of monomeric GTPases called Rab proteins, such as Rab3A (exocytosis marker), Rab4A (recycling marker), Rab5B (endosome marker), and Rab7B (late endosome marker). As shown in Fig. 2B, these Rab proteins co-fractionated with DJ-1. However, mitochondrial respiratory complex proteins (Complex I subunit NDUFB8, Complex II subunit 30 kDa, Complex III subunit Core 2, and ATP synthase (Complex V) subunit α), which are mitochondrial markers, and the Golgi apparatus protein GM130, were not concentrated in the synaptic vesicle fraction (LP2) (Fig. 2D). The amount of each fraction was quantified and expressed as a percentage for the estimated amount of whole brain protein. The percentage of the P1 fraction was $2.69 \pm 0.20\%$, and DJ-1 was present in the nucleus, even though it was small. The percentages of P2′, LS1, LP1, LS2, and LP2, were $19.07 \pm 0.80\%$, $3.71 \pm 0.08\%$, $17.58 \pm 2.36\%$, $2.46 \pm 0.11\%$, and $0.75 \pm 0.19\%$, respectively (Fig. 2E). The amount of protein in the LP2 fraction was much less than that of the whole brain. DJ-1 IR of each fraction was quantified and shown as a percentage of each IR to total immunoreactivities. The percentage of DJ-1 IR of each fraction was $9.82 \pm 0.22\%$ (P2′), $13.19 \pm 0.07\%$ (LS1), $6.18 \pm 0.20\%$ (LP1), $12.54 \pm 0.50\%$ (LS2), and $5.43 \pm 1.08\%$ (LP2) (Fig. 2F).

DJ-1 localized on synaptic vesicles associated with synaptophysin and Rab3A

DJ-1 distributed with synaptic vesicles in the mouse brain (Fig. 2C). To elucidate the vesicle localization of DJ-1, the LS1 fraction containing synaptic vesicles and cytosol from mouse brain was further fractionated by sucrose density gradients centrifugation. Synaptophysin, VAMP2, synaptotagmin, and several Rab proteins were seen in fractions 9–18, and therefore, synaptic vesicles were collected in these fractions (Fig. 3A, B). Otherwise, the immunoreactivities of the synaptic vesicle markers were absent in fractions 1–8, suggesting that they were cytosolic fractions. The distribution of DJ-1 displayed biphasic peaks of both cytosolic fractions (fractions 1–8) and vesicle fractions (fractions 12–14). Coincidentally, the peak of DJ-1 IR agreed with the latter peak of synaptophysin and Rab3A (Fig. 3A, B). To further investigate the colocalization between DJ-1 and synaptic vesicles in neurons, primary cortical neuronal cells obtained from mouse brain were double-stained for DJ-1, and for synaptophysin or Rab3A. DJ-1 immunostaining appeared as punctate structures in the cytosol, axon, and synaptic terminals. DJ-1 was found to partly colocalize with synaptophysin and Rab3A, which play important roles in exocytosis (Edelmann et al., 1995; Handley et al., 2007) (Fig. 3C).

To gain further insight into the vesicle localization of DJ-1, immunoisolation was performed, as previously described (Burre et al., 2007; Morciano et al., 2005), with the LS1 fraction containing synaptic cytosol and vesicles from the mouse brain (Fig. 4A). To remove the nonspecifically interacting material, the LS1 fraction was treated with antibody-linked magnetic beads (Dyna-beads), which are cross-linked with normal rabbit or mouse IgG, and then the beads were removed. It was confirmed that DJ-1 and synaptophysin were not lost under this condition (Fig. 4B). Pre-cleaned LS1 was incubated with the Dyna-beads cross-linked with the DJ-1 antibodies, and then the vesicle isolates containing DJ-1 were subjected to immunoblotting with the DJ-1 antibody. Interestingly, synaptophysin and VAMP2 also localized with the DJ-1-associated vesicles (Fig. 4C). HSP70, which is known as a nuclear and cytosolic protein (Daugaard et al., 2007), was not isolated by this procedure (Fig. 4C). This indicates that the synaptic vesicle fraction was not contaminated with the cytosolic fraction. Therefore, this suggests that DJ-1, synaptophysin, and VAMP2 might localize on the surface of the same vesicle. In addition, it was further investigated whether DJ-1 directly interacts with synaptophysin and/or VAMP2. The LS1 fraction treated with RIPA buffer was immunoprecipitated with pull-down beads cross-linked

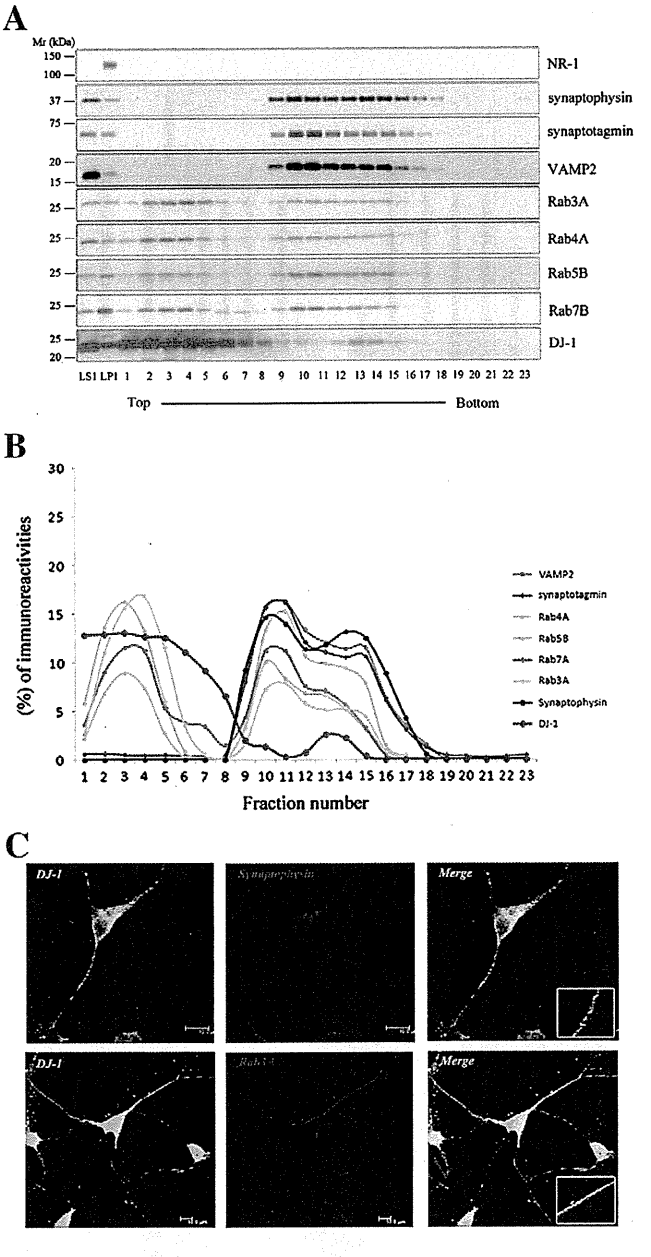

Fig. 3. DJ-1 associates with synaptic vesicles and colocalizes with synaptophysin and Rab3A. (A) The LS1 fraction was layered on top of a linear sucrose density gradient ranging from 0.2–2.0 M sucrose dissolved in HEPES buffer. Fractions were collected and 15 μl of each fraction were subjected to SDS–PAGE followed by immunoblotting using various markers. (B) Using the results from panel A, IR of each fraction was quantified and graphed as a percentage of each IR to the total immunoreactivities in each marker. DJ-1 had a biphasic profile of the immunoreactivities in fractions 1–8 and fractions 12–14, which indicated that there was some cytosolic fraction and some vesicle fractions. The peak of DJ-1 IR was in agreement with the latter peak of synaptophysin and Rab3A. (C) Primary cortical neurons from the mouse brain were fixed, permeabilized, and immunostained with DJ-1 antibody, and double-stained for synaptophysin and Rab3A. DJ-1 overlapped with synaptophysin and Rab3A. Scale bars = 10 μm.

with the synaptophysin antibody. It was found that VAMP2 interacts with synaptophysin as previous studies had reported (Baumert et al., 1989; Edelmann et al., 1995; Trimble et al., 1988). Immunoblotting with DJ-1 antibodies did not reveal endogenous DJ-1 in the resultant immunoprecipitates (Fig. 4C), whereas, endogenous synaptophysin and VAMP2 were not immunoprecipitated with the DJ-1 antibody.

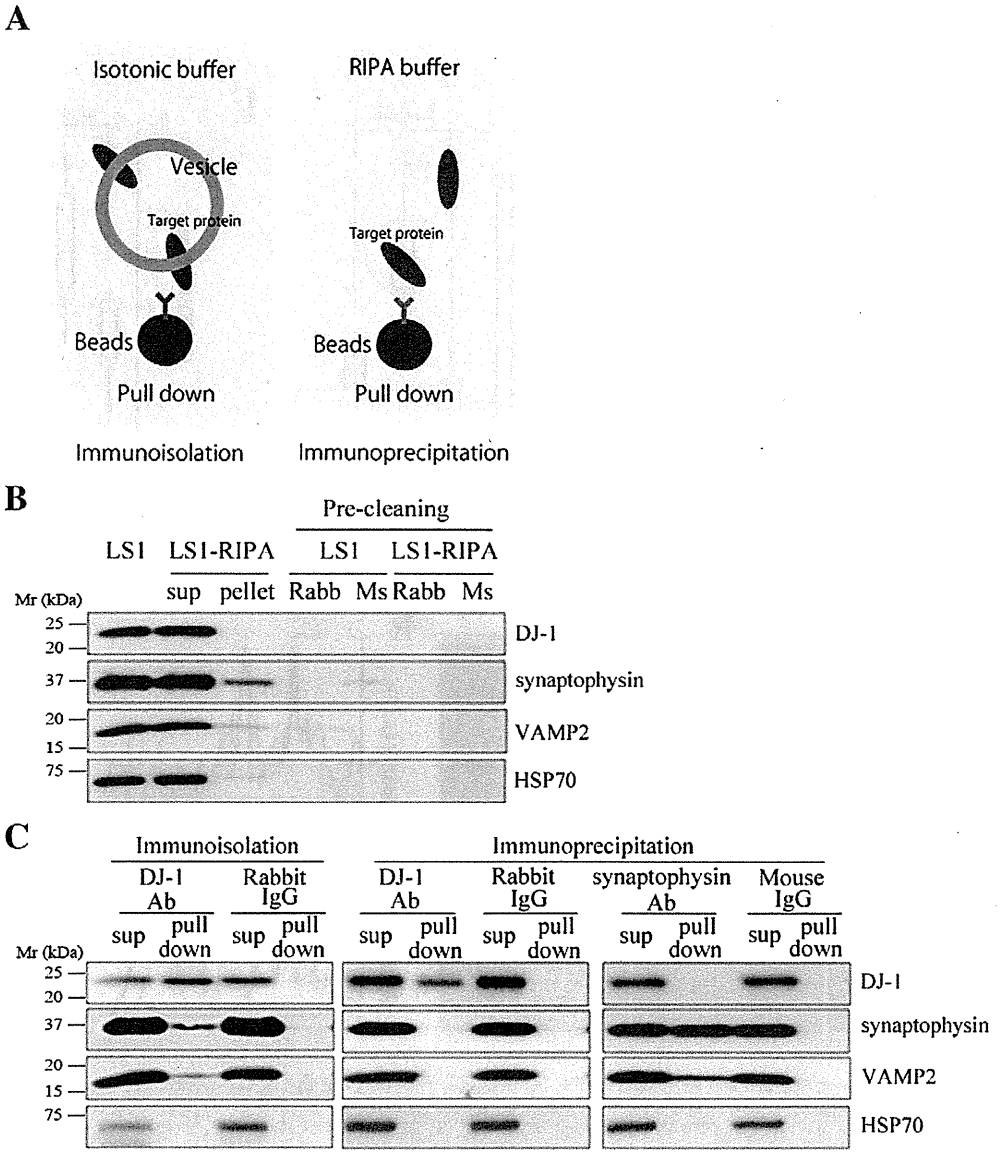

Fig. 4. DJ-1 cannot directly interact with synaptophysin and VAMP2, but associates with the same synaptic vesicles. (A) Image of immunoisolation and immunoprecipitation. Immunoisolation was used to pull down the target protein from the subcellular organelles (synaptic vesicle) from the homogenate, which was reacted with the isotonic buffer. Meanwhile, immunoprecipitation was used to pull down the target protein from the homogenate, which reacted with the buffer containing the detergent in order to examine the direct interactions between proteins. These methods were then used to assess the protein localized on the subcellular organelles with the target protein. (B) The LS1 fraction was first pre-cleaned. To remove nonspecifically-binding material, the LS1 fraction was treated with Dyna-beads cross-linked with normal rabbit or mouse IgG. It was confirmed that the targeting proteins were not lost in this reaction. (C) Sucrose buffer or RIPA buffer extracts of the mouse brain synaptic vesicle fractions were immunoisolated or immunoprecipitated using Dyna-beads coated with each antibody. Immunoisolates, immunoprecipitates and their corresponding supernatants were subjected to SDS–PAGE followed by immunoblotting using antibodies against the indicated proteins. Synaptophysin and VAMP2 were immunoisolated using Dyna-beads coated with the DJ-1 antibody, but they were not immunoprecipitated with the same bead slurry. Sup, supernatant.

Consequently, this proves that DJ-1 cannot directly interact with synaptophysin and VAMP2, but colocalizes with them on the same vesicles.

FRET analyses were performed to examine whether DJ-1 interacts with synaptophysin. We confirmed that FRET occurred between CFP–VAMP2, considered as positive control and synaptophysin-YFP (Pennuto et al., 2002). However, FRET was detected only in a small proportion of HeLa cells expressing CFP–DJ-1 and synaptophysin-YFP (Fig. 5A). $FRET_C$ median values with CFP–VAMP2, CFP–DJ-1, and CFP alone for more than 20 cells, were expressed as 0.363, 0.0413, and 0.0163, respectively (Fig. 5B). 293F cells expressing CFP–VAMP2 or CFP–DJ-1 and synaptophysin-YFP were also subjected to fluorescence lifetime flow cytometry, and fluorescence lifetimes of more than 10,000 cells in each sample were measured. Again, FRET efficiency observed between DJ-1 and synaptophysin was substantially lower than that between VAMP2 and synaptophysin, but significantly higher than that of the control (Fig. 5C). Confocal microscopic analyses revealed that CFP–DJ-1 also merged with synaptophysin-YFP. This pattern is similar to the colocalization between CFP–VAMP2 and synaptophysin-YFP (Fig. 5D, E). These results indicate that DJ-1 is able to localize with synaptophysin-positive vesicles and may interact with synaptophysin in living cells.

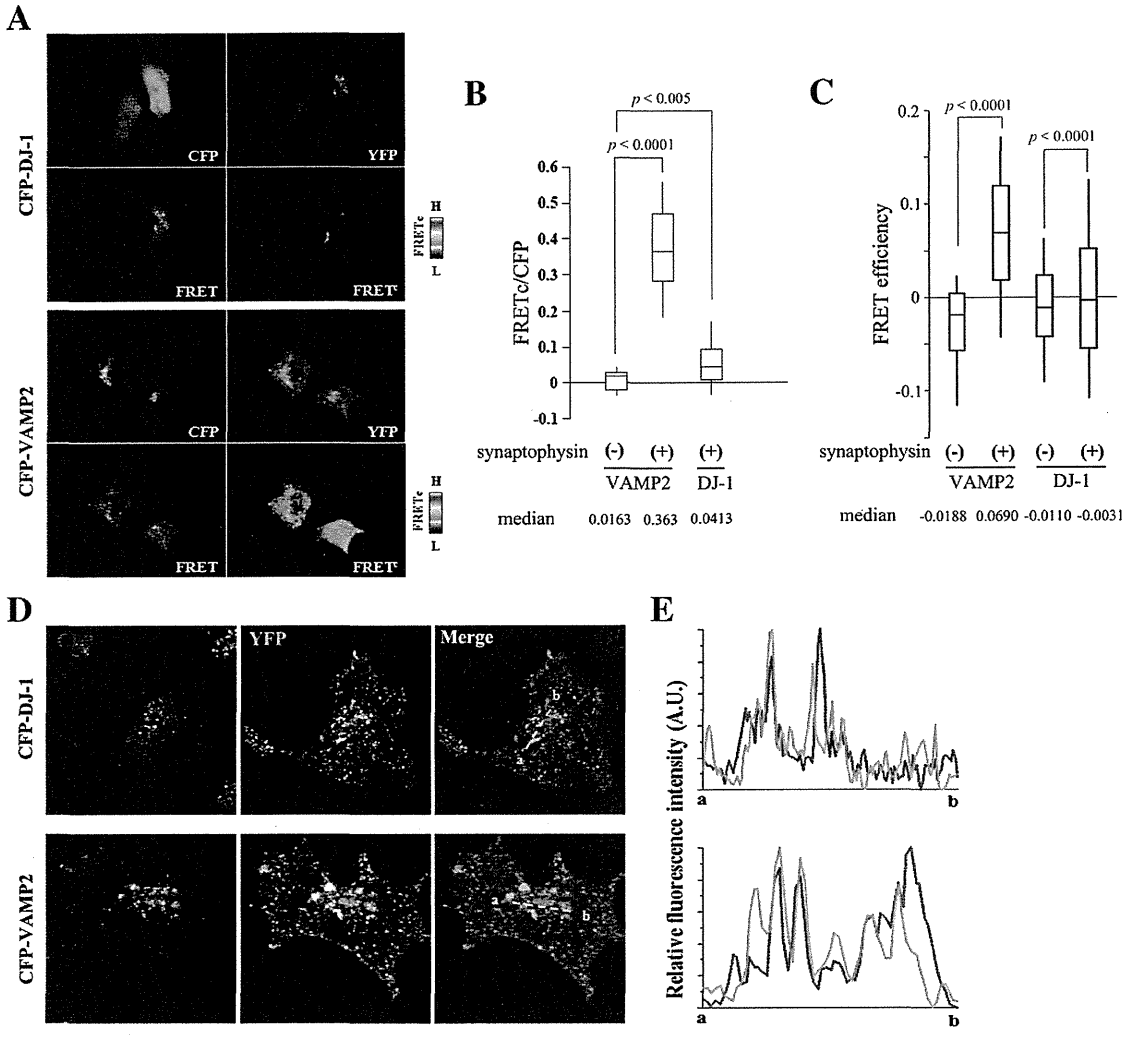

Fig. 5. FRET occurred in HeLa cells expressing CFP–DJ-1 and synaptophysin-YFP. (A) HeLa cells expressing CFP–DJ-1 or CFP–VAMP2, and synaptophysin-YFP were subjected to microscopic analysis as described in Materials and methods, and representative images are shown. FRET was detected in HeLa cells expressing CFP–VAMP2 and synaptophysin-YFP. FRET occurred in a small proportion of HeLa cells expressing CFP–DJ-1 and synaptophysin-YFP. (B) $FRET_C$ values calculated for each cells were plotted in the box and whisker plot. Representative data from three independent experiments are shown. The highest and lowest boundaries of the box represent the 25th and 75th percentiles, respectively, and whiskers above and below the box designate the 10th and 90th percentiles, respectively; the line within the box indicates the median value. (C) 293F cells expressing CFP–DJ-1 or CFP–VAMP2 and synaptophysin-YFP were subjected to fluorescence lifetime flow cytometry as described in Materials and methods. Fluorescence lifetimes of more than 10,000 cells in every sample were plotted in the box and whisker plot, where the highest and lowest boundaries of the box represent the 25th and 75th percentiles, respectively, and whiskers above and below the box designate the 10th and 90th percentiles, respectively; the line within the box indicates the median value. (D) Cells were imaged on a confocal laser microscope and representative images are shown. In a small proportion of cells CFP–DJ-1 merged with synaptophysin-YFP. CFP–VAMP2 colocalized with synaptophysin-YFP. (E) Fluorescence intensities of CFP (red) and YFP (green), along with the line in the merged image in (D), were plotted from a to b. Note that overlapping peaks indicate colocalization.

DJ-1 directly associates with membranes

The results from the immunocytochemical and biochemical experiments indicated that DJ-1 localizes in membranous structures, but it is unclear how DJ-1 associates with membranes. To address this issue, the effect of ionic strength on the association between DJ-1 with membranes was examined. PC12 cells were fractionated by centrifugation at 100,000*g* to pellets and supernatants, corresponding to membrane and cytosolic fractions, respectively. DJ-1 was collected in both the cytosol and the membranes. Although DJ-1 does not shift from the membrane to the cytosol regardless of high salt conditions, non-ionic detergent Triton X-100 solubilizes DJ-1 in a way similar to that of the transferrin receptor (Tfn-R) with a transmembrane domain (Fig. 6A). Meanwhile, parkin, which associates with lipid rafts (Fallon et al., 2002; Kubo et al., 2001), did not dissociate from the membrane by solubilization with Triton X-100 (Fig. 6A).

To characterize membrane-binding of DJ-1 protein, an in vitro binding assay using PC12 cells was employed as previously described (Kubo et al., 2005). In this assay, DJ-1 was found to be bound to purified plasma membranes. Treatment of plasma membranes purified from PC12 cells with Proteinase K (PK) for 60 min at 30 °C did not alter the localization of DJ-1 (Fig. 6C). We confirmed that digestion in PK for 60 min largely eliminated the protein as detected by silver staining (Fig. 6B).

L166P mutation affects membrane-binding ability

To investigate the pathogenicity of the mutant DJ-1 on membrane-binding ability, a membrane-binding assay was performed using the GST recombinant protein of wild type DJ-1 (GST–DJ-1 WT) and various pathogenic mutants. To eliminate the effects of endogenous DJ-1, DJ-1 knockout (KO) mice were used for this experiment. Synaptosomes from

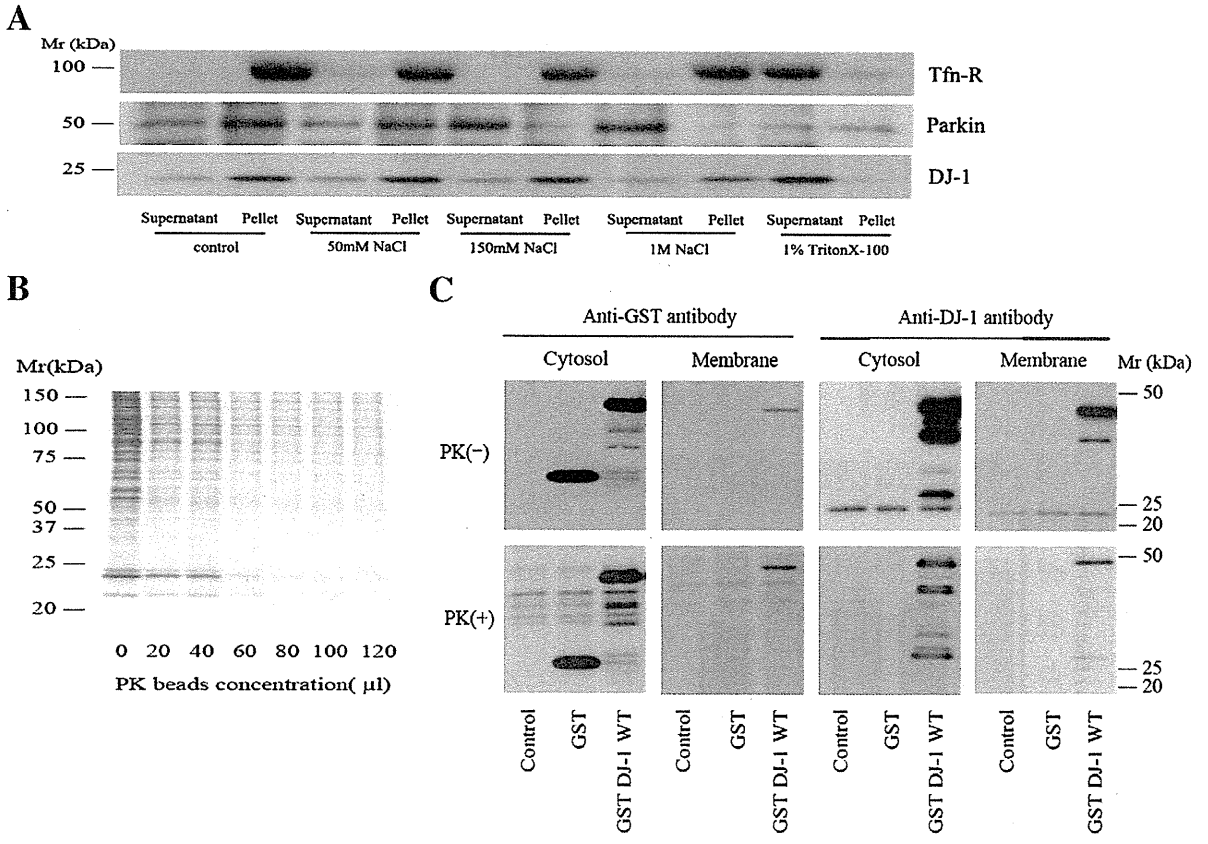

Fig. 6. Endogenous DJ-1 associates with cytosol and plasma membrane in PC12 cells. (A) Effects of various salt concentrations and non-ionic detergent on solubilization of DJ-1, Parkin, and transferrin receptor (Tfn-R). DJ-1 was concentrated in both the cytosol and membrane fractions of PC12 cells in the detergent-free isotonic buffer (control). DJ-1 did not shift from the membrane to the cytosol with increasing salt concentration, whereas Parkin relocalized from the membrane to cytosol, and Tfn-R remained in the pellet. However, DJ-1 did release from the membrane after being subjected to Triton X-100. Tfn-R was readily solubilized in this condition as well. Parkin remained in the pellet. Equal volumes of each of the fractions were loaded, followed by immunoblotting. (B) Silver staining of PC12 membranes treated with Proteinase K (PK) for 60 min at 30 °C showed a progressive loss of detectable membrane proteins with increasing PK concentration. (C) Recombinant DJ-1 wild type (WT), fused at its N terminus to the GST protein, was reacted with PC12 membranes or PK-treated membranes for 60 min at 30 °C. The GST-tagged protein, which served as a negative control, was also reacted. The reacted samples were centrifuged and divided into supernatant and pellet. Both supernatant and pellet were subjected to SDS–PAGE followed by immunoblotting. Anti-GST antibody detected the GST–DJ-1 WT recombinant protein band in the pellet fraction, whereas the GST-tagged protein was not detected in the pellet fraction. GST–DJ-1 WT recombinant protein directly associated with the plasma membrane in the in vitro assay.

DJ-1 KO mice were incubated with the GST–DJ-1 WT recombinant protein, or the GST–DJ-1 mutant recombinant proteins. Bound proteins were separated by centrifugation at 260,000g for 2 h. Compared with WT, the L166P mutant exhibited less binding to the synaptic membranes obtained from DJ-1 KO mice. However, there were no apparent differences between other pathogenic mutants and the WT in their membrane-binding property (Fig. 7A, B).

To further analyze the subcellular localization of various pathogenic DJ-1 mutants, HeLa cells were transfected with various DJ-1 mutants, as well as WT DJ-1 as control. M26I, A104T, and D149A showed diffuse and punctate distribution, similar to WT. By comparison, L166P exhibited localization near the plasma membrane (Fig. 7C).

Discussion

The overarching goal of this study was to determine the endogenous localization and membrane binding ability of DJ-1 and to elucidate potential differences in its properties between WT and pathogenic mutants. Immunocytochemistry for endogenous DJ-1 showed that the labeled structures distributed diffusely and displayed punctate staining. In the biochemical experiments, endogenous DJ-1 localized to the Golgi apparatus, cellular membranes, and synaptic vesicles which contain synaptophysin and Rab proteins. The GST–DJ-1 protein was found to be bound to cultured cellular membrane and mouse synaptosomes, as evidenced in the in vitro binding assay. Furthermore, this study shows that compared with WT, the L166P mutant exhibited less binding to the synaptic vesicles from DJ-1 KO mice.

Although several studies have reported on the mitochondrial localization of DJ-1 in cultured cells and mouse brains (Bonifati et al., 2003; Canet-Aviles et al., 2004; Miller et al., 2003; Zhang et al., 2005), Bandopadhyay et al. reported that they could not confirm the mitochondrial localization of endogenous DJ-1 in mouse primary astrocytes and hippocampal neurons (Bandopadhyay et al., 2004). Olzmann et al. described that DJ-1 localizes to the striatal axons and pre-synaptic terminals, suggesting a role for DJ-1 in dopaminergic neurotransmission (Olzmann et al., 2007). Zhang et al. also showed that DJ-1 was found in a synaptic-enriched fraction, however, they did not mention whether DJ-1 is associated with membrane trafficking (Zhang et al., 2005). In our experiments, DJ-1 partly localized to the synaptic cytosol, vesicles and membranes in the synaptic terminals of the mouse brain. However, a small portion of endogenous DJ-1 was located in mitochondria under steady state conditions, consistent with previous reports (Bandopadhyay et al., 2004; Nural et al., 2009). Thus, the present findings of endogenous DJ-1 localization provide evidence that DJ-1 may be associated with synaptic vesicles.

DJ-1 has the same distribution as members of the monomeric GTPases family called Rab proteins, known through biochemical

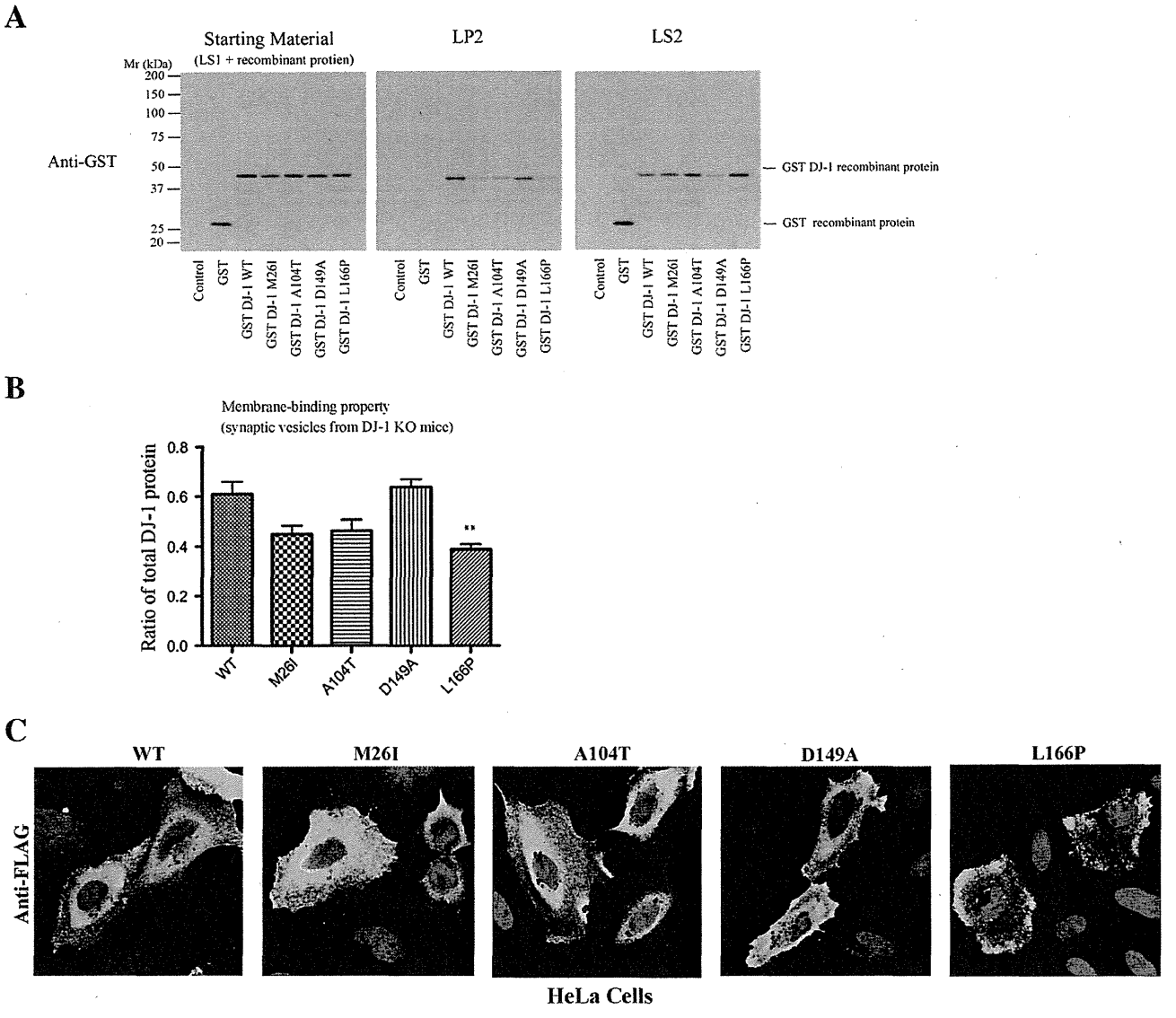

Fig. 7. Pathogenic DJ-1 mutants can bind membranes in the in vitro assay. (A) The LS1 fraction of DJ-1 KO mouse was reacted for 20 min at 30 °C with 500 nM GST recombinant protein, WT, or various mutants. Each of the bound proteins was divided into an LP2 fraction (synaptic vesicles) and an LS2 fraction (synaptic cytosol) by ultra-centrifugation at 260,000g for 2 h at 4 °C. The samples were subjected to SDS–PAGE followed by immunoblotting. The A104T, L166P, and M26I mutations also had lower bands corresponding to synaptic vesicles (LP2 fraction), compared with WT and D149A DJ-1. The GST-tagged protein, which served as a negative control was not detected. (B) Quantitative data from three independent experiments showed that the L166P mutant had reduced binding ability with the synaptic membrane. Immunoreactivity was quantified and expressed as percentage of bound (LP2) to total DJ-1 protein (LP2 + LS2). The data were plotted as the mean ± SEM. $^{**}P<0.001$ vs. WT, one-way ANOVA with Dunnett's Multiple Comparison Test. The other mutations were not statistically significant. The data were analyzed by GraphPad Prism (GraphPad Software, Inc.). (C) HeLa cells were transfected with expression vectors for FLAG-DJ-1 WT, M26I, A104T, D149A, or L166P. After 24 h, immunocytochemistry assay was performed on the cells. WT and the mutants, with the notable exception of the L166P mutant, appeared to have diffused subcellular distribution. WT was localized to the cytosol and in punctate spots. Similar results were obtained for mutants DJ-1, except for L166P. L166P localized near the plasma membrane.

studies as proteins associated with membrane trafficking (Harald Stenmark, 2001). DJ-1 may possibly associate with one and/or some of the Rab proteins. Actually, DJ-1 was found to partly colocalize with Rab3A by double-staining. Rab3A associates with immature secretory granules from the trans-Golgi network and has positive roles in exocytosis (Handley et al., 2007). Considering the colocalization between DJ-1 and Rab3A at synaptic terminals, DJ-1 could be involved in the vesicular trafficking system in such processes as exocytosis. Actually, DJ-1 KO mice exhibited altered synaptic functions, such as less sensitivity to the inhibitory effects of D2 auto receptor stimulation (Goldberg et al., 2005).

How can DJ-1 participate in synaptic vesicle transport? Corresponding with the results of the in vitro immunoisolation and immunoprecipitation assay, DJ-1 was found to not bind synaptophysin and VAMP2 directly, but DJ-1 localized with the synaptophysin and VAMP2-associated vesicles. In the in vivo FRET assay, a small portion of DJ-1 interacted with synaptophysin. Therefore, part of DJ-1 may be fairly close to synaptophysin and VAMP2. Neurotransmitter exocytosis involves sequential association of many synaptic proteins. Vesicular fusion, which is the central process of exocytosis, is mediated by the regulation of soluble N-ethylmaleimide sensitive factor (NSF) attachment protein receptor complexes, including VAMP2, syntaxin and synaptosome-associated protein 25 kDa (SNAP-25). These proteins interact with each other and play a critical role in the step between vesicle docking and fusion (Edelmann et al., 1995). Interestingly, several steps of vesicle fusion are regulated by molecular chaperones such as

NSF, 70 kDa heat-shock cognate protein, and cysteine-string protein (Zinsmaier and Bronk, 2001). DJ-1 is supposed to be a member of the DJ-1/YajL/Pfpl superfamily, which function as molecular chaperones, and in RNA binding and hydrolase activity (Wei et al., 2007). Therefore, DJ-1 may participate in the regulation of neurotransmitter release as a molecular chaperone on synaptic vesicles.

From the results of the membrane-binding assay, DJ-1 was found to directly associate with membranes without an intermediary protein. Considering that the membrane binding of DJ-1 was not influenced by high-salt conditions, DJ-1 does not appear to associate with the membrane through electrostatic interactions such as ionic bonds, hydrogen bonds, and van der Waals attraction. Incubation with the non-ionic detergent Triton X resulted in release of DJ-1. This may mean that DJ-1 might prefer not to associate with lipid rafts, which are microdomains on membranes containing GM1 ganglioside, GPI anchor proteins, and several other membrane proteins (Edidin, 2003; Legler et al., 2005). Additionally, DJ-1 has no obvious amino acid sequences that serve as a targeting signal and transmembrane domains based on computer analysis (Kyte, 1982). Therefore, DJ-1 probably attaches to membranes through hydrophobic interactions.

Membrane proteins can bind to the lipid bilayer in various ways (Bruce Alberts, 2002; Lomize et al., 2007). In the proteins, peripheral membrane proteins temporarily adhere to the surface of the membrane. Some of them interact with membranes via an amphipathic α helix in the cytosolic monolayer (Bruce Alberts et al., 2002; Lomize et al., 2007). Based on crystal analyses, DJ-1 consists of a six-stranded parallel β-sheet sandwiched by eight α-helices and with a β-hairpin on one end and a three-stranded anti-parallel β-sheet on the opposite end (Anderson and Daggett, 2008; Wilson et al., 2003). Although the structure of DJ-1 is similar to that of a bacterial protein Pfp1, which is known as a cysteine protease, one major difference is the presence of an additional α-helix (helix αH) at the C terminus of DJ-1. The function of the helix αH is assumed to play a role in dimerization in combination with the helix αG (Honbou et al., 2003; Wilson et al., 2003). L166P is at the middle of the helix αG and is associated with significant structural deformations in this helix (Wilson et al., 2003). Additionally, the L166P mutant influences the membrane-binding property and disrupts the DJ-1 dimer (Anderson and Daggett, 2008). Therefore, we suspect that the α helices at the C terminus of DJ-1 are also able to function in membrane binding.

We also showed that the L166P mutant exhibits less binding to the synaptic vesicles from the DJ-1 KO mice compared with the WT, using the membrane-binding assay with the WT and various pathogenic mutations. Considering that the membrane-binding abilities of other mutations had no statistical difference with WT, it is presumed that the helix αG at the C terminus of DJ-1 associates with membrane binding. Actually, the results of the immunocytochemistry analysis of WT or mutants of DJ-1-overexpressing cells also revealed that the L166P mutant altered intracellular localization.

Based on our experiments, we believe that the association between DJ-1 and synaptic vesicles may contribute to the pathomechanisms in *PARK7*-linked PD. The previous studies have reported that α-synuclein, Parkin, and LRRK2 also localize to synaptic membranes and are associated with membrane trafficking (Abeliovich et al., 2000; Fallon et al., 2002; Hatano et al., 2007; Kahle et al., 2000; Kubo et al., 2001; Shin et al., 2008). Abnormality of membrane trafficking could be considered an important pathomechanism of PD as a common pathway. Further research may elucidate how DJ-1 associates with synaptic vesicles and why the loss of DJ-1 causes dopaminergic neuronal degeneration in PD.

Conclusions

This study is the first report showing the precise localization of endogenous DJ-1. We showed that DJ-1 colocalized with the Golgi apparatus proteins GM130 and the synaptic vesicle proteins synaptophysin and Rab3A. Although wild-type DJ-1 protein directly associated with membranes without an intermediary protein, the pathogenic L166P mutation of DJ-1 exhibited less binding to synaptic vesicles. Our findings indicate that DJ-1 associates with membranous organelles including synaptic membranes for its normal function.

Acknowledgments

We thank Norihiro Tada, Sachiko Ujiie, Sumihiro Kawajiri, Yuanzhe Li, Yoko Imamichi, and Akiko Egashira (Juntendo University). We are grateful to Shigeo Okabe and Shinji Tanaka (the Department of Cellular Neurobiology Graduate School of Medicine University of Tokyo) for providing synaptophysin-YFP and pCAGGS-CFP vectors. This work was supported by grants for Scientific Research Priority Areas (to N. H.), Scientific Research B (to N. H.), Scientific Research C (to S. K.), Young Scientists B (to T. H. and S. I.) from the Japanese Ministry of Education, Culture, Sports, Science and Technology of Core Research for Evolutional Science and Technology in the Japan Science and Technology (to N. H.), and the Research for the Future program of the Japan Society for the Promotion of Science, a Takeda Science Foundation (to S. K.).

References

Abeliovich, A., et al., 2000. Mice lacking alpha-synuclein display functional deficits in the nigrostriatal dopamine system. Neuron 25, 239–252.
Anderson, P.C., Daggett, V., 2008. Molecular basis for the structural instability of human DJ-1 induced by the L166P mutation associated with Parkinson's disease. Biochemistry 47, 9380–9393.
Bandopadhyay, R., et al., 2004. The expression of DJ-1 (PARK7) in normal human CNS and idiopathic Parkinson's disease. Brain 127, 420–430.
Baumert, M., et al., 1989. Synaptobrevin: an integral membrane protein of 18,000 daltons present in small synaptic vesicles of rat brain. EMBO J. 8, 379–384.
Bonifati, V., et al., 2003. Mutations in the DJ-1 gene associated with autosomal recessive early-onset parkinsonism. Science 299, 256–259.
Bruce Alberts, A.J., Julian, Lewis, Martin, Raff, Keith, Roberts, Peter, Walter (Eds.), 2002. Molecular Biology of the Cell, fourth edition. Garland Science, a member of the Taylor & Francis Group, New York.
Burre, J., et al., 2007. Immunoisolation and subfractionation of synaptic vesicle proteins. Anal. Biochem. 362, 172–181.
Canet-Aviles, R.M., et al., 2004. The Parkinson's disease protein DJ-1 is neuroprotective due to cysteine-sulfinic acid-driven mitochondrial localization. Proc. Natl. Acad. Sci. U.S.A. 101, 9103–9108.
Daugaard, M., et al., 2007. The heat shock protein 70 family: highly homologous proteins with overlapping and distinct functions. FEBS Lett. 581, 3702–3710.
Edelmann, L., et al., 1995. Synaptobrevin binding to synaptophysin: a potential mechanism for controlling the exocytotic fusion machine. EMBO J. 14, 224–231.
Edidin, M., 2003. The state of lipid rafts: from model membranes to cells. Annu. Rev. Biophys. Biomol. Struct. 32, 257–283.
Fallon, L., et al., 2002. Parkin and CASK/LIN-2 associate via a PDZ-mediated interaction and are co-localized in lipid rafts and postsynaptic densities in brain. J. Biol. Chem. 277, 486–491.
Fearnley, J.M., Lees, A.J., 1991. Ageing and Parkinson's disease: substantia nigra regional selectivity. Brain 114 (Pt 5), 2283–2301.
Goldberg, M.S., et al., 2005. Nigrostriatal dopaminergic deficits and hypokinesia caused by inactivation of the familial Parkinsonism-linked gene DJ-1. Neuron 45, 489–496.
Gordon, G.W., et al., 1998. Quantitative fluorescence resonance energy transfer measurements using fluorescence microscopy. Biophys. J. 74, 2702–2713.
Handley, M.T., et al., 2007. Differential dynamics of Rab3A and Rab27A on secretory granules. J. Cell Sci. 120, 973–984.
Harald Stenmark, V.M.O., 2001. The Rab GTPase family. Genome Biol. 2, 3007.1–3007.7.
Hatano, T., et al., 2007. Leucine-rich repeat kinase 2 associates with lipid rafts. Hum. Mol. Genet. 16, 678–690.
Hatano, T., et al., 2009. Pathogenesis of familial Parkinson's disease: new insights based on monogenic forms of Parkinson's disease. J. Neurochem. 111, 1075–1093.
Hell, J. W. a. J., R., 1998. Preparation of synaptic vesicles from mammalian brain. Celis, J.E. (Eds). San Diego.
Honbou, K., et al., 2003. The crystal structure of DJ-1, a protein related to male fertility and Parkinson's disease. J. Biol. Chem. 278, 31380–31384.
Kahle, P.J., et al., 2000. Subcellular localization of wild-type and Parkinson's disease-associated mutant alpha-synuclein in human and transgenic mouse brain. J. Neurosci. 20, 6365–6373.
Kim, R.H., et al., 2005. DJ-1, a novel regulator of the tumor suppressor PTEN. Cancer Cell 7, 263–273.
Kubo, S., et al., 2005. A combinatorial code for the interaction of alpha-synuclein with membranes. J. Biol. Chem. 280, 31664–31672.
Kubo, S., et al., 2001. Parkin is associated with cellular vesicles. J. Neurochem. 78, 42–54.
Kyte, J.a.D.,.R.F., 1982. A simple method for displaying the hydropathic character of a protein. J. Mol. Biol. 157, 105–132.

Lee, S.J., et al., 2003. Crystal structures of human DJ-1 and *Escherichia coli* Hsp31, which share an evolutionarily conserved domain. J. Biol. Chem. 278, 44552–44559.
Legler, D.F., et al., 2005. Differential insertion of GPI-anchored GFPs into lipid rafts of live cells. FASEB J. 19, 73–75.
Lomize, A.L., et al., 2007. The role of hydrophobic interactions in positioning of peripheral proteins in membranes. BMC Struct. Biol. 7, 44.
Miller, D.W., et al., 2003. L166P mutant DJ-1, causative for recessive Parkinson's disease, is degraded through the ubiquitin–proteasome system. J. Biol. Chem. 278, 36588–36595.
Morciano, M., et al., 2005. Immunoisolation of two synaptic vesicle pools from synaptosomes: a proteomics analysis. J. Neurochem. 95, 1732–1745.
Niki, T., et al., 2003. DJBP: a novel DJ-1-binding protein, negatively regulates the androgen receptor by recruiting histone deacetylase complex, and DJ-1 antagonizes this inhibition by abrogation of this complex. Mol. Cancer Res. 1, 247–261.
Nural, H., et al., 2009. Dissembled DJ-1 high molecular weight complex in cortex mitochondria from Parkinson's disease patients. Mol Neurodegener. 4, 23.
Olzmann, J.A., et al., 2007. Selective enrichment of DJ-1 protein in primate striatal neuronal processes: implications for Parkinson's disease. J. Comp. Neurol. 500, 585–599.
Pennuto, M., et al., 2002. Fluorescence resonance energy transfer detection of synaptophysin I and vesicle-associated membrane protein 2 interactions during exocytosis from single live synapses. Mol. Biol. Cell 13, 2706–2717.
Shin, N., et al., 2008. LRRK2 regulates synaptic vesicle endocytosis. Exp. Cell Res. 314, 2055–2065.
Shinbo, Y., et al., 2005. DJ-1 restores p53 transcription activity inhibited by Topors/p53BP3. Int. J. Oncol. 26, 641–648.
Taira, T., et al., 2004a. Co-localization with DJ-1 is essential for the androgen receptor to exert its transcription activity that has been impaired by androgen antagonists. Biol. Pharm. Bull. 27, 574–577.
Taira, T., et al., 2004b. DJ-1 has a role in antioxidative stress to prevent cell death. EMBO Rep. 5, 213–218.
Takahashi, K., et al., 2001. DJ-1 positively regulates the androgen receptor by impairing the binding of PIASx alpha to the receptor. J. Biol. Chem. 276, 37556–37563.
Trimble, W.S., et al., 1988. VAMP-1: a synaptic vesicle-associated integral membrane protein. Proc. Natl. Acad. Sci. U.S.A. 85, 4538–4542.
Wei, Y., et al., 2007. Identification of functional subclasses in the DJ-1 superfamily proteins. PLoS Comput. Biol. 3, e10.
Wilson, M.A., et al., 2003. The 1.1-A resolution crystal structure of DJ-1, the protein mutated in autosomal recessive early onset Parkinson's disease. Proc. Natl. Acad. Sci. U.S.A. 100, 9256–9261.
Yokota, T., et al., 2003. Down regulation of DJ-1 enhances cell death by oxidative stress, ER stress, and proteasome inhibition. Biochem. Biophys. Res. Commun. 312, 1342–1348.
Zhang, L., et al., 2005. Mitochondrial localization of the Parkinson's disease related protein DJ-1: implications for pathogenesis. Hum. Mol. Genet. 14, 2063–2073.
Zinsmaier, K.E., Bronk, P., 2001. Molecular chaperones and the regulation of neurotransmitter exocytosis. Biochem. Pharmacol. 62, 1–11.

SAGE-Hindawi Access to Research
Parkinson's Disease
Volume 2011, Article ID 473640, 5 pages
doi:10.4061/2011/473640

Clinical Study

Nonmotor Symptoms in Patients with *PARK2* Mutations

Asako Yoritaka,[1] Yumi Shimo,[1] Yasushi Shimo,[1] Yuichi Inoue,[2] Hiroyo Yoshino,[1] and Nobutaka Hattori[1]

[1] *Department of Neurology, Juntendo University School of Medicine, 2-1-1 Hongo, Bunkyo-ku, Tokyo 113-8421, Japan*
[2] *Japan Somnology Center, Neuropsychiatric Research Institute, 1-24-10 Yoyogi, Shibuya-ku, Tokyo 151-0053, Japan*

Correspondence should be addressed to Asako Yoritaka, ayori@juntendo.ac.jp

Received 14 October 2010; Accepted 16 December 2010

Academic Editor: Irena Rektorova

Decreased ^{123}I-meta-iodobenzylguanidine (MIBG) uptake in MIBG myocardial scintigraphy, olfactory dysfunction, and rapid eye movement (REM) sleep behavior disorder (RBD) are considered useful early indicators of Parkinson disease. We investigated whether patients with *PARK2* mutations exhibited myocardial sympathetic abnormalities using MIBG scintigraphy, olfactory dysfunction using the Sniffin' Sticks olfactory test, and RBD using polysomnography. None of the examined patients had RBD, and all except 1 patient exhibited an increase in the olfactory threshold. Moreover, one of the oldest patients exhibited impairment in identification and discrimination. Of 12 patients with *PARK2* mutations, 4 patients, who were older than patients without abnormal uptake, exhibited decreased MIBG uptake. The results obtained in this study suggest that some patients with *PARK2* mutations have increased thresholds of olfactory function and myocardial sympathetic dysfunction as nonmotor symptoms.

1. Introduction

Mutations in the *parkin* gene (*PARK2*) are considered to be the predominant cause of early-onset Parkinson disease particularly when the family history is compatible with autosomal recessive inheritance [1]. This condition is characterized by early onset of disease, usually before the age of 40 years, dystonia, sleep benefit, early complications from levodopa treatment, and slow progression. *Parkin*-associated tremor-dominant parkinsonism includes a spectrum of late-onset disorders without manifestations of foot dystonia, hyperreflexia, diurnal fluctuations, sleep benefit, or early susceptibility to levodopa-induced dyskinesia [2]. Therefore, patients with *PARK2* mutations are often clinically indistinguishable from those with sporadic Parkinson's disease (PD).

PD patients exhibit decreased myocardial uptake of meta-iodobenzylguanidine (MIBG) during ^{123}I-MIBG myocardial scintigraphy—a finding indicative of cardiac sympathetic denervation [3]. Olfactory impairment, an early symptom of PD, occurs in more than 70% of patients with PD [4]. Rapid eye movement (REM) sleep behavior disorder (RBD) is characterized by a loss of normal skeletal muscle atonia and complex motor activity, specifically during REM sleep associated with dream mentation. Thirty-eight percent of RBD patients aged ≥ 50 years were eventually diagnosed with PD [5]; therefore, RBD may serve as an early indicator of PD.

Here, we examined nonmotor symptoms in patients with *PARK2* mutations.

2. Methods

Mutation of the parkin gene was confirmed by gene analysis [1]. Eight women and 7 men possessed mutations in the *PARK2* gene: cases 1, 2, 3, 8, and 13 carried homozygous-deletions, and the remaining carried heterozygous mutations or deletions (Table 1). Clinical findings and medications are shown in Table 1.

The MIBG study involved 6 women and 7 men (mean (SD) age, 58.5 (11.4) years) with *PARK2* mutations: 5 subjects had homozygous deletions, and 8 had heterozygous mutations or deletions. Patients had parkinsonism for a mean (SD) period of 22.0 (11.59) years (range, 10–44 years). When MIBG scintigraphy was performed, the patients were not medicated with monoamine oxidase B (MAOB) inhibitors, selective serotonin reuptake inhibitors, or antidepressant drugs. Data was collected by E CAM at 30 minutes and 3 hours after injection of ^{123}I-MIBG

Table 1: Clinical findings and medication of patients with PARK2 mutation.

Case	1	2	3	4	5	6	7	8	9	10	11	12	13	14
Age sex	71 F	55 M	46 M	41 F	38 M	36 F	76 M	70 M	63 M	61 F	61 F	60 F	57 M	44 F
Parkin	exon 2–4 homo deletion	exon 5 homo deletion	exon 6, 7 homo deletion	exon 6 hetero deletion	exon 4, intron 4 accepter site, A → G	exon 10 hetero mutation	exon 10 hetero mutation	exon 2 homo-deletion	exon 2, 3, 4 hetero deletion	exon 2, 3 hetero deletion	exin 4 hetero deletion	exon 3, 4 hetero deletion	exon 2, 3, 4 homo-deletion	exon 5 hetero deletion
On set	61	28	28	27	18	20	65	45	33	29	47	16	45	34
Disease duration	10	27	18	14	20	16	11	28	36	34	14	44	12	10
Family history	–	+	+	–	–	+	+	–	–	+	–	+	+	+
Hoehn & Yahr stage on	2	2	2	1	1.5	2	2	3	3	3	3	3	1	1
Rigidity*	1	1	0	1	2	0	1	0	0	1	0	0	0	0
Tremor*	1	0	0	1	0	0	1	1	0	0	0	0	0	0
Hesitation*	0	1	1	0	0	2	0	1	1	2	2	1	0	0
Wearing-off	+	+	+	–	+	+	–	+	+	+	+	–	+	–
Dementia	–	–	–	–	–	+**	–	–	–	–	–	–	–	–
Hallucination	–	–	–	–	–	+	–	–	–	–	+	–	–	–
Sleep violent behavior	–	–	–	–	–	–	–	–	–	–	–	–	–	–
Constipation	+***	–	–	–	–	–	–	–	–	–	+	–	–	–
Levodopa	700 mg	600 mg	600 mg	300 mg	400 mg	300 mg	–	300 mg	500 mg	995 mg	800 mg	200 mg	450 mg	–
Agonist non-ergot	pramipexole 1.5 mg	pramipexole 4.5 mg	pramipexole 3 mg	ropinirole 9 mg	pramipexole 1.5 mg	ropinirole 12 mg	pramipexole 4.5 mg	–	pramipexole 0.75 mg	pramipexole 1.5 mg	pramipexole 2.25 mg	ropinirole 16 mg	–	pramipexole 1.5 mg
Agonist ergot	–	pergolide 2.25 mg	–	–	cabergoline 4 mg	–	–	–	–	–	–	–	cabergoline 2 mg	–
Selegiline	–	5 mg	–	–	10 mg	5 mg	–	–	–	–	5 mg	–	2.5 mg	–
Entacapone	–	400 mg	600 mg	–	300 mg	600 mg	–	–	400 mg	–	–	–	–	–
Trihexyphenidyl	–	–	–	–	3 mg	–	–	5 mg	–	–	–	–	–	–
Amantadine	300 mg	150 mg	300 mg	–	300 mg	–	–	–	150 mg	200 mg	100 mg	300 mg	–	–

DID: dopa induced dyskinesia.
*UPDRS mean score **Thalamotomy ***no medication.

(MyoMIBG-I 123 injection, 111 MBq; FUJIFILM RI Pharma Co. Ltd.). The cut-off ratio of the heart to mediastinum (H/M) uptake ratio of ^{123}I-MIBG in our hospital was set at 1.45.

The olfactory function and polysomnography (PSG) study involved 3 women and 3 men (mean (SD) age, 47.8 (13.2) years) with *PARK2* mutations (Table 1).

The mean olfactory function scores of the PD patients and 10 age-matched Japanese controls, who were evaluated for comparison with patients with *PARK2* mutations, were determined by the Sniffin' Sticks test. Mean age of the controls without neurological disease or dementia was 46.0 (15.3) years (range, 39–79 years). The PD patients (mean age, 69.6 (6.6) years; range, 60–89 years; not age matched to patients with *PARK2* mutations) fulfilled the UK Brain Bank criteria for possible or probable clinical PD, with Hoehn-Yahr stages II and III without dementia.

Olfactory testing was examined by following 3 components. Olfactory threshold and odor discrimination and identification were investigated in 3 separate substrates using standardized Sniffin' Sticks [6]. Sniffin' Sticks are commercially available felt-tip pens.

Odor Thresholds. The olfactory threshold subset consisted of 16 Sniffin' Stick triplets with different concentrations of *n*-butanol. Three sticks were presented to the subject in randomized order. Two contained only the solvent and the third the odorant at a particular dilution. The subjects were tasked to identify the stick with the odorant.

Odor Discrimination. In the odor discrimination subset, 16 Sniffin' Stick triplets were presented in randomized order. Two pens contained the same odorant and the third a different odorant. The task was to identify the stick that had the different smell.

Odor Identification. The third subtest consisted of 16 single sticks and assessed the ability to identify an odor. Using a multiple-choice task, identification of individual odorants was performed from a list of 4 descriptors.

RBD was confirmed by studying the patients' clinical history and video-PSG findings (International Classification of Sleep Disorders, 2nd edition) [7].

Informed consent was obtained from patients with *PARK2* mutations, and patients with PD, and normal volunteers.

The data was statistically analyzed using SPSS ver.11 for Windows.

3. Results

The mean H/M uptake ratio of ^{123}I-MIBG scintigraphy in *PARK2* patients was 1.79 (0.31) in the early phase and 1.75 (0.51) in the delayed phase (Table 2). However, a 58-year-old woman, with a 10-year disease duration and orthostatic hypotension and constipation without myocardial damage, exhibited accelerated MIBG elimination (H/M ratio: early, 1.23; delayed, 1.15). Three patients (cases 2, 7, and 12) had exhibited slightly decreased uptake in the delayed phase.

The Sniffin' Sticks test revealed a slight olfactory dysfunction with the following mean scores in examined *PARK2* patients (Table 3): threshold score, 6.1 (1.6) ($P < .05$ when compared with controls); odor discrimination score, 10.0 (2.4); odor identification score, 10.1 (4.8) (no significant differences when compared to controls). Odor discrimination and identification functions were not impaired in any of the patients with *PARK2* mutations, except in patient 1. In the Japanese examined normative controls, the mean olfactory function scores were as follows: threshold score, 8.0 (1.3); discrimination score, 11.9 (2.4); identification score, 10.9 (2.0); in PD patients, these mean scores were 2.2 (6.6), 6.1 (2.5), and 5.1 (1.8), respectively.

PSG did not reveal tonic responses in the mentalis and tibialis muscles during REM (Table 3). Twitching of the tibialis muscle was observed in 2 patients. None of the patients with *PARK2* mutations met the ICSD-II criteria for RBD.

4. Discussion

Decreased ^{123}I-MIBG uptake was observed clearly in 1 patient with *PARK2* mutations who had autonomic dysfunction. Early phase myocardial uptake of MIBG in all of the other patients showed no decrease, and patients had no autonomic dysfunction. Similar to our study, in a previous study [8], 1 of 4 patients with *PARK2* mutations with a 12-year disease duration and unclear autonomic dysfunction exhibited decreased uptake of ^{123}I-MIBG. Additionally, 3 patients in our study who showed decreased ^{123}I-MIBG uptake were slightly older than the other patients, although a significance in mean age (63.0 (9.1) versus 55.9 (10.8); $P > .05$) did not exist. Estorch et al. and Tsuchimochi et al. reported that the uptake of ^{123}I-MIBG decreased with age, suggesting that aging could affect patients with *PARK2* mutations [9, 10]. Decreased myocardial uptake of MIBG is considered to indicate the presence of alpha-synuclein aggregates in the axons in PD [11]. In MIBG-myocardial scintigraphy, the H/M ratio of patients with *PARK2* mutations was reported to be within the range of the normal controls [12]. Moreover, postmortem examination of patients with *PARK2* mutations revealed that tyrosine hydroxylase immunoreactive nerve fibers in the epicardium were well preserved [13]. These findings might reflect normal functioning myocardial sympathetic nerve terminals in patients with *PARK2* mutations. MIBG scintigraphy might be a marker for alpha-synuclein in patients with *PARK2* mutations; however, there are no pathological reports on the presence of Lewy bodies in patients with *PARK2* mutations exhibiting decreased MIBG uptake.

Olfactory impairment is a nonmotor symptom of PD. We found that the olfactory threshold was slightly higher in patients with *PARK2* mutations than in controls. The oldest woman in our study, who did not have dementia, exhibited the highest degree of olfactory impairment. Although in self-completed questionnaire study, 3 of 16 patients with *PARK2* mutation had loss of taste/smell [14]. However, in previous

Table 2: The findings of ^{123}IMIBG myocardial scintigraphy in PARK2 patients.

Case	1	2	3	5	7	8	9	10	11	12	13	14	Average ± SD
Examined age	65	55	46	41	76	70	63	61	61	60	57	44	58.3 ± 10.5
Early H/M	2.27	1.64	1.91	1.75	1.52	2.05	1.75	1.66	1.23	1.75	1.62	2.35	1.79 ± 0.31
Delay H/M	2.14	1.33	1.67	1.93	1.34	2.93	1.65	1.54	1.15	1.40	1.60	2.35	1.75 ± 0.51

H/M: the heart to mediastinum uptake ratio of ^{123}IMIBG.

Table 3: Olfactory function by Sniffin' sticks and PSG study in patients with PARK2 mutation, controls, and Parkinson's disease.

Case	1	2	3	4	5	6	*PARK2* total ($n = 6$)	Control ($n = 10$)	Parkinson's disease ($n = 15$)
Age	71	55	46	41	38	36	47.8 ± 13.2	46.0 ± 15.3	69.6 ± 6.6
Sniffin' sticks Test									
Threshold test	4.5	6.3	6.3	5.8	5.0	9.0	6.1 ± 1.6	8.0 ± 1.3*	2.2 ± 2.3**
Discrimination test	8.0	9.0	12.0	14.0	9.0	8.0	10.0 ± 2.4	11.9 ± 2.4	6.1 ± 2.5
Identification test	1.0	13.0	10.0	14.0	13.0	10.0	10.1 ± 4.8	10.9 ± 2.0	5.1 ± 1.8
PSG findings									
Apnea index (times/H)	10.1	22.5	1.2	0.4	1.0	2.1			
Hypopnea index (times/H)	2.2	14.0	4.7	0.3	1.9	9.4			
Apnea Hypopnea index (times/H)	12.3	36.5	5.9	0.8	3.0	11.4			
Arousal index (times/H)	16.0	39.8	37.7	13.4	14.3	11.1			
Respiratory arousal index (times/H)	5.5	27.3	4.6	0.2	1.6	3.3			
PLM index(times/H)	7.8	0.0	7.7	0.0	29.5	0.0			
PLM arousal index(times/H)	0.0	0.0	5.3	0.0	2.8	0.0			
REM sleep twitching on TA muscle	−	+	−	+	−	−			

H/M: theheart to mediastinum uptake ratio, NE: not examined.
PLM: periodic limb movements, TA: tibialis anterior.
*t-test: compared with *PARK2* patients $P < .05$.
**t-test: compared with *PARK2* patients and control $P < .01$.

studies, individuals with *PARK2* mutations were found to have normal olfactory function [15, 16]. The discrepancy between our results and previous ones may be because previous studies used the Pennsylvania Smell Identification Test, which does not include the threshold test. In Kahn's study [15], the odor identification score did not significantly differ between patients with *PARK2* mutations and controls, although this did not necessarily imply that the threshold score was normal in the patients.

PSG did not reveal RBD in any of our patients. However, in a study by Kumru et al., 6 of 10 patients had RBD [17]. We cannot explain this discrepancy, but we hypothesize that it may be due to the differences in patient mean age between the 2 studies. Some of our patients with *PARK2* mutations have twitching in the tibialis muscle; therefore, the possibility that they will eventually develop RBD cannot be ruled out. Neuropathological studies on patients with *PARK2* mutations have revealed neuronal loss and gliosis in the pars compacta of the substantia nigra and in the locus coeruleus [18]. However, these studies have not described the state of the subcoeruleus nucleus, which is considered the primary site affected in RBD.

The results obtained in this study suggest that some patients with *PARK2* mutations have increased thresholds of olfactory function and myocardial sympathetic dysfunction as nonmotor symptoms. We might show that the nonmotor symptoms of *PARK2* were impaired heterogeneously.

Author Contributions'

A. Yoritaka was responsible for conception, execution of research projects, statistical analysis, writing of first draft and review and critique; Yasushi Shimo was responsible for execution of research project; Yumi Shimo and Y. Inoue were responsible for execution of research project (PSG study); H. Yoshino was responsible for gene analysis; N. Hattori was responsible for conception and organization of research project.

References

[1] T. Kitada, S. Asakawa, N. Hattori et al., "Mutations in the parkin gene cause autosomal recessive juvenile parkinsonism," *Nature*, vol. 392, no. 6676, pp. 605–608, 1998.

[2] M. M. Mouradian, "Recent advances in the genetics and pathogenesis of Parkinson disease," *Neurology*, vol. 58, no. 2, pp. 179–185, 2002.

[3] S. Orimo, E. Ozawa, S. Nakade, T. Sugimoto, and H. Mizusawa, "^{123}I-metaiodobenzylguanidine myocardial scintigraphy in Parkinson's disease," *Journal of Neurology Neurosurgery and Psychiatry*, vol. 67, no. 2, pp. 189–194, 1999.

[4] C. H. Hawkes, B. C. Shephard, and S. E. Daniel, "Olfactory dysfunction in Parkinson's disease," *Journal of Neurology Neurosurgery and Psychiatry*, vol. 62, no. 5, pp. 436–446, 1997.

[5] C. H. Schenck, S. R. Bundlie, and M. W. Mahowald, "Delayed emergence of a parkinsonian disorder in 38% of 29 older, men initially diagnosed with idiopathic rapid eye movement sleep behavior disorder," *Neurology*, vol. 46, no. 2, pp. 388–393, 1996.

[6] T. Hummel, B. Sekinger, S. R. Wolf, E. Pauli, and G. Kobal, "'Sniffin' sticks'. Olfactory performance assessed by the combined testing of odor identification, odor discrimination and olfactory threshold," *Chemical Senses*, vol. 22, no. 1, pp. 39–52, 1997.

[7] American Academy of Sleep Medicine, *International Classification of Sleep Disorders: Diagnostic and Coding Manual*, American Academy of Sleep Medicine, Westchester, Ill, USA, 2nd edition, 2005.

[8] A. Quattrone, A. Bagnato, G. Annesi et al., "Myocardial ^{123}metaiodobenzylguanidine uptake in genetic Parkinson's disease," *Movement Disorders*, vol. 23, no. 1, pp. 21–27, 2008.

[9] M. Estorch, I. Carrió, L. Berná, J. López-Pousa, and G. Torres, "Myocardial iodine-labeled metaiodobenzylguanidine 123 uptake relates to age," *Journal of Nuclear Cardiology*, vol. 2, no. 2, pp. 126–132, 1995.

[10] S. Tsuchimochi, N. Tamaki, S. Shirakawa et al., "Evaluation of myocardial distribution of iodine-123 labeled metaiodobenzylguanidine (^{123}I-MIBG) in normal subjects," *Kakuigaku*, vol. 31, no. 3, pp. 257–264, 1994.

[11] S. Orimo, T. Uchihara, A. Nakamura et al., "Axonal α-synuclein aggregates herald centripetal degeneration of cardiac sympathetic nerve in Parkinson's disease," *Brain*, vol. 131, no. 3, pp. 642–650, 2008.

[12] M. Suzuki, N. Hattori, S. Orimo et al., "Preserved myocardial [^{123}I] metaiodobenzylguanidine uptake in autosomal recessive juvenile parkinsonism: first case report," *Movement Disorders*, vol. 20, no. 5, pp. 634–636, 2005.

[13] S. Orimo, T. Amino, M. Yokochi et al., "Preserved cardiac sympathetic nerve accounts for normal cardiac uptake of MIBG in PARK2," *Movement Disorders*, vol. 20, no. 10, pp. 1350–1353, 2005.

[14] G. Kägi, C. Klein, N. W. Wood et al., "Nonmotor symptoms in Parkin gene-related parkinsonism," *Movement Disorders*, vol. 25, no. 9, pp. 1279–1284, 2010.

[15] N. L. Khan, R. Katzenschlager, H. Watt et al., "Olfaction differentiates parkin disease from early-onset parkinsonism and Parkinson disease," *Neurology*, vol. 62, no. 7, pp. 1224–1226, 2004.

[16] D. Verbaan, S. Boesveldt, S. M. van Rooden et al., "Is olfactory impairment in Parkinson disease related to phenotypic or genotypic characteristics?" *Neurology*, vol. 71, no. 23, pp. 1877–1882, 2008.

[17] H. Kumru, J. Santamaria, E. Tolosa et al., "Rapid eye movement sleep behavior disorder in parkinsonism with PARKIN mutations," *Annals of Neurology*, vol. 56, no. 4, pp. 599–603, 2004.

[18] H. Mori, T. Kondo, M. Yokochi et al., "Pathologic and biochemical studies of juvenile parkinsonism linked to chromosome 6q," *Neurology*, vol. 51, no. 3, pp. 890–892, 1998.